Micelle kinetics of photoswitchable surfactants: Self-assembly pathways and relaxation mechanisms

Victoria Ariel Bjørnestad, Xinmeng Li, Christophe Tribet, Reidar Lund, Michele Cascella

Journal of Colloid and Interface Science 646 (2023) 883–899

Contents lists available at ScienceDirect

Journal of Colloid And Interface Science

journal homepage: www.elsevier.com/locate/jcis

Regular Article

Micelle kinetics of photoswitchable surfactants: Self-assembly pathways and relaxation mechanisms

Victoria Ariel Bjørnestad [a], Xinmeng Li [a], Christophe Tribet [b], Reidar Lund [a,*], Michele Cascella [a,*]

[a] Hylleraas Centre for Quantum Molecular Sciences, Department of Chemistry, University of Oslo, Sem Sælands vei 26, Oslo, 0371, Norway
[b] PASTEUR, Département de Chimie, École Normale Supérieure, PSL University, Sorbonne Université, CNRS, Paris, 75005, France

ARTICLE INFO

Keywords:
Azobenzene
Photoswitch
Cationic surfactant
Micelle kinetics
Molecular dynamics
SAXS

ABSTRACT

Hypothesis: A key question in the kinetics of surfactant self-assembly is whether exchange of unimers or fusion/fission of entire micelles is the dominant pathway. In this study, an isomerizable surfactant is used to explore fundamental out-of-equilibrium kinetics and mechanisms for growth and dissolution of micelles.
Experiments: The kinetics of cationic surfactant 4-butyl-4'-(3-trimethylammoniumpropoxy)-phenylazobenzene was studied using molecular dynamics simulations. The fusion and exchange processes were investigated using umbrella sampling. Equilibrium states were validated by comparison with small-angle X-ray scattering data. The photo-isomerization event was simulated by modifying the torsion potential of the photo-responsive group to emulate the *trans*-to-*cis* transition.
Findings: Micelle growth is dominated by unimer exchange processes, whereas, depending on the conditions, dissolution can occur both through fission and unimer expulsion. Fusion barriers increase steeply with the aggregation number making this an unlikely pathway to equilibrium for micelles of sizes that fit with the experimental data. The barriers for unimer expulsion remain constant and are much lower for unimer insertion, making exchange more likely at high aggregation. When simulating photo-conversion events, both fission and a large degree of unimer expulsion can occur depending on the extent of the out-of-equilibrium stress that is put on the system.

1. Introduction

The self-assembly processes of surfactant molecules are critical in many applications, such as detergency [1], food preparations [2], new drug delivery systems [3] and biochemical protocols [4]. Knowledge of the kinetics of self-assembly is thus important for many technological applications, but so far most of the work related to this has been focused on conventional surfactants [5].

One of the key questions is whether morphological changes in micellar systems, such as growth and dissociation, are dominated by unimer exchange between the micelles and solvent or by fusion/fission of entire micelles. The theory of step-wise growth of micelles by Aniansson and Wall [6,7], which assumes that all morphological changes in micelles occur via unimer exchange is so far the most developed theoretical framework to describe the dynamic processes in micellar systems. The theory is based on the Becker-Döring equations, which assume that nucleation processes can be modelled only with step-wise addition/removal of the unimers [8,9]. This theory is generally accepted for describing the fast processes that equilibrate the micellar aggregation number after an initial destabilization of the system, but it also assumes that a change in the number of micelles must be the result of a complete formation/dissolution of micelles from/to their unimer state.

Fusion and fission events, however, should also be considered as candidates in micelle equilibration [10–14]; for example, Pool and Bolhuis suggested a *replication mechanism* for micelle formation whereby a growing micelle can split to give two resultant aggregates that can continue to grow [15]. Several other computational studies have also found fusion and fission events to play important roles in micellar kinetics for a range of different types of surfactants, especially when the system is far from equilibrium [16–22].

Among the vast chemical library of scaffolds, the class of light-responsive surfactants are of particular interest for their ability to transition between different aggregation states without the involvement of external environmental factors like temperature, solvent, pH

* Corresponding authors.
E-mail addresses: reidar.lund@kjemi.uio.no (R. Lund), michele.cascella@kjemi.uio.no (M. Cascella).

https://doi.org/10.1016/j.jcis.2023.05.057
Received 31 January 2023; Received in revised form 19 April 2023; Accepted 9 May 2023
Available online 15 May 2023

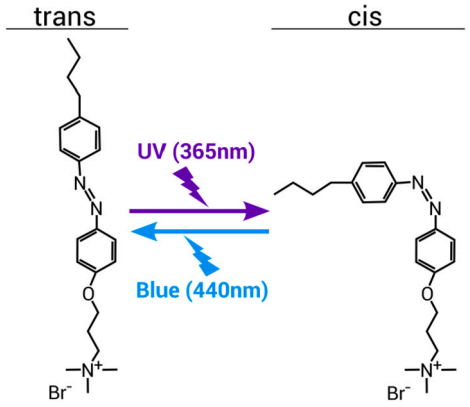

Fig. 1. The chemical structure of 4-butyl-4'-(3-trimethylammoniumpropoxy)-phenylazobenzene (AzoTMA) is illustrated along with the *trans*-to-*cis* isomerization that occurs upon illumination at specific wavelengths.

etc. Such control can be very useful in many applications, ranging from environmental cleanup to targeted drug delivery [23]. 4-butyl-4'-(3-trimethylammoniumpropoxy)-phenylazobenzene (AzoTMA), whose chemical structure is drawn in Fig. 1, is a representative of photo-responsive surfactants that was optimized to maximize the shift of the critical micellar concentration (CMC) upon exposure to light [24]. AzoTMA has previously attracted attention for its ability to tune the surface tension [25], and to make photo-controllable foams [26] and lipid-surfactant systems [27]. Nonetheless, the motivation for studying the aggregation kinetics of this particular surfactant goes well beyond its intrinsic interest for technological applications. In fact, at a more fundamental level, AzoTMA offers an ideal playground to investigate the interplay between surfactant polarity and aggregation dynamics without changing the chemistry of the system. This is possible thanks to the evidence that photo-sensitive surfactants undergo a fast and reversible change in their structural hydrophilic-lipophilic balance, which can lead to large deviations in the micellar shape and aggregation number [28]. AzoTMA *trans-to-cis* isomerization occurs upon illumination with UV-light [29]. While the *trans* isomer is non-polar, the *cis*-configuration has a large dipole moment across the azo-linkage, and the AzoTMA structure is near to be optimal for maximizing variation of surface tension upon the *trans-cis* conversion [24]. The CMC of the AzoTMA surfactant in pure water has been found to vary from 1.9 mM for the dark adapted state to 2.8 mM in the UV-illuminated state [30], although perfect conversion could not be achieved at experimental conditions. In presence of a chaotropic agent, like in a 17% DMF solution, the CMC has been found to vary from 9.3 mM to close to 14 mM upon UV-illumination.

Unlike for well-investigated conventional amphiphiles [31,10], to date there are only a few computational studies on photo-controllable surfactants. Notable examples that have all been published quite recently are studies on the interaction of photo-switchable azobenzene surfactants with DNA in the context of controlling DNA packaging [32,33], the effect of photo-switching on reverse micelles of an azobenzene-surfactant [34], and also the effect of the micellar environment on the photo-isomerization event in a single surfactant [35].

Most events of micelle kinetics are considered to be too rare for observation using all-atom molecular dynamics (MD) simulations, and so studies have mostly been limited to studying the initial fast aggregation of unimers. By combining molecular dynamics simulations with enhanced sampling methods such as umbrella sampling, however, rare events such as fusion/fission and unimer insertion/expulsion in fully formed micelles can also be studied. In this work, we have used this approach to investigate the aggregation dynamics of AzoTMA. The aggregation kinetics and effects of photo-isomerization on photo-controllable micellar systems are particularly interesting due to their potential to form states that are far from equilibrium, and to the authors' knowledge this paper constitutes the first attempt at studying these processes with molecular dynamics. The use of simulations to study photo-controllable surfactants also allow full control over the photo-isomerization process by eliminating the possibility of observing effects that actually arise from the experimental conditions such as incomplete illumination volume and concurrent heating of the system. Previous research has rather focused on design and proof of concept of macroscopic control [36,26,25,24,37,28], and experimental conditions are usually restrained in their possibilities to investigate the microscopic kinetics of structural evolution of these responsive systems. Here we show that by using a combination of molecular dynamics together with validation of the structures towards experimental small angle X-ray scattering (SAXS) data, we can elucidate the mechanisms that are at work in these systems. The results provide insight into the different kinetic processes that can occur upon isomerization of photoresponsive surfactant micelles which should be considered in applications involving these types of assemblies.

The kinetics of AzoTMA was previously investigated by Lund et al. using time-resolved SAXS [30]. To validate the structure of the equilibrated aggregates, we have done direct comparisons of the structures obtained from the simulations with the experimental SAXS data from that study. Computed spectra were obtained by calculating the scattering intensity as a function of the modulus of the momentum transfer vector, Q, using the explicit-solvent method of Hub and coworkers [38,39]. The aggregation kinetics was explored by simulating the *trans*-surfactant, where the different mechanisms for micellar growth were investigated by performing umbrella sampling of the fusion event and the single surfactant exchange. Finally, the kinetics of the photo-conversion of equilibrated micelles were explored by simulating the *trans-cis* transition for different percentages of isomerization and the results were compared with the experimental data. Two different solvent conditions were tested: pure water and 30% dimethylformamide (DMF) solution, where the latter will cause a reduction in the hydrophobic effect and thereby a higher CMC value. From the results we can identify unimer exchange as the dominant process for micellar growth, whereas a reduction in the aggregation number as observed upon isomerization of the surfactant can be caused by either unimer expulsion or micellar fission depending on the amount of out-of-equilibrium stress put on the system.

2. Methods

2.1. System and simulation details

The OPLS-AA force field [40] was used to parameterize all the molecular moieties present in the simulations, which were performed with GROMACS version 2018.4 [41]. The molecular model in all our simulations employs the all-atom OPLS force-field to describe the solute moieties and DMF [42], and the TIP4P model for water [40]. The molecular models for AzoTMA were built starting using conventional OPLS rules for atom types and charge groups. The *cis*-, *trans*- conformations are taken into account by the torsional potential at the –N=N– moiety. The topologies are provided as Supplementary information. The leap-frog algorithm with a time-step of 2 fs was used for the integration of the equations of motion. Bond stretching involving hydrogen atoms were constrained by the LINCS algorithm [43]. All systems were simulated in the isothermal-isobaric ensemble at a constant temperature of 300 K and a pressure of 1 Bar, using the CSVR thermostat [44] and the Parrinello-Rahman barostat algorithms [45]. The particle mesh Ewald (PME) was used to calculate the long-range electrostatics, while short-range non-bonded interactions were cut off at 1.0 nm, and periodic boundary conditions applied in all directions. Coordinates were saved every 10 ps.

2.2. Simulations of aggregation from dispersed state

For simulations of initial aggregation of AzoTMA, molecules corresponding to a concentration of 205 mM were placed randomly in two different box sizes of 9x9x9 and 11x11x11 nm^3, respectively. The boxes were then solvated with water and bromide ions were added to neutralize the systems. The fully assembled systems were then relaxed by steepest descent minimization, followed by equilibration in the NVT ensemble for 200 ns to stabilize the temperature at 298 K and then in the NPT ensemble for 200 ns to stabilize the pressure to 1 bar. For simulations of initial aggregation in the presence of different percentages of DMF, random placement of AzoTMA molecules was followed by the random insertion of a number of DMF molecules corresponding to 17%, 30% and 50% into the empty space of the box before solvation and placement of ions; otherwise the same procedure as previously described was followed. A detailed description of the computational protocol can be found in Appendix A, with Table A.1 describing the setup for the two different simulated systems.

2.3. Umbrella sampling simulations for fusion of micelles

Umbrella sampling was performed on the fusion/fission event of two micelles and on the fusion/fission of one monomer and one micelle, also referred to as a single molecular exchange event. The starting micelles were selected from the simulations of the initial aggregation from a random state or from the simulations of the fusion of larger micelles which were equilibrated as described in sections 2.4, A.2 (with Table A.2 giving an overview of the different equilibrated micelles), and A.3. A detailed overview of where the different micelles used in the umbrella sampling simulation were acquired from can be found in Table A.3. Starting configurations for the micelles in the different windows of the simulation were generated by placing the center of mass (COM) of the micelles progressively further together followed by energy minimization and position restrained temperature and pressure equilibration. This procedure has been described in detail in Appendix A. For the monomer-micelle fusion, the starting structures were generated by placing the center for mass of the free surfactant molecule progressively towards the COM of the micelle with the TMA-group facing away from the COM of the micelle, followed by the same minimization and equilibration procedure as above. Sampling windows were chosen such that the window spacing was 0.1 nm up to 2 nm COM separation and 0.2 nm beyond 2 nm of COM separation for the simulation of micelle-micelle fusion. For the monomer-micelle fusion simulations, the window spacing was 0.1 nm at all separations. Molecular dynamics simulations with the COM constrained were performed using an harmonic potential of 1000 kJ mol^{-1} nm^{-2} for 10 ns for each window, where the first ns was discarded from the analysis. Further simulation times are not found to change the results outside the margin of error of the umbrella simulations. The weighted histogram analysis (WHAM) method in GROMACS as implemented by Hub et al. [46] was used to analyze the trajectories, and the histograms were checked for sufficient overlap to be able to give convergence. Statistical error was calculated using the bootstrapping technique with 100 bootstraps.

2.4. Simulation of fusion event and formation of equilibrated micelles of specific aggregation numbers

To generate structures of higher aggregation number than what was achieved during the initial aggregation simulations, the fusion event was simulated by choosing sampling windows at the left side of the peak of the free energy curves as found in section 2.3. A normal production run without the umbrella constraints was then run to give the equilibrated, fused aggregate, as detailed in A.2. For the simulations of the single micelles in water, the cubic box sizes were 10x10x10, 11x11x11, 12x12x12 and 15x15x15 nm^3 for the aggregation number 15, 30, 60 and 120 respectively (corresponding to concentrations of 24 mM, 37 mM, 57 mM and 59 mM, respectively). Completion of fusion of the P = 30, 60 and 120 aggregates was evaluated as when the radius of gyration (R_g) of the fused micelle had stabilized, which can be seen in Fig. A.10. The degree of mixing was indicated by the separation of the center of mass of the surfactants originating from the two different micelles, (d). Micelles that were fused and considered adequately mixed ($d < R_g$) were considered to be equilibrated.

2.5. Trans-cis switching simulations

The *trans-cis* photo-isomerization event was simulated by modifying the torsional potential of the C–N=N–C group by introducing an energy barrier at the *trans*-state where the dihedral angle is 180°, approximating the energy of the excited state as described by Heinz et al. [47]. As seen from Fig. A.13 the change in geometry of the molecules occurs within the first picoseconds, while the relaxation of the system takes about 10 ps, both observations in accordance with what was found previously [47]. Different quantum yields were simulated by choosing AzoTMA-molecules at random in the appropriate percentage and applying the modified potential only for those molecules.

2.6. Comparison with small angle X-ray scattering data

The small angle X-ray scattering data was collected by Lund et al. at the ID02 instrument at the European Synchrotron Radiation Facility (ESRF) for a previous experimental study on the AzoTMA micelle kinetics [30]. AzoTMA with a bromide counterion had been synthesized as described in reference [26]. The surfactant was dissolved in Millipore water to give a concentration of 14.6 mM. Two-dimensional scattering patterns were measured in 10 frames of 20 ms both for the AzoTMA sample and for a pure water sample with a fast read-out, low-noise CCD detector (FReLoN) at an X-ray wavelength of 0.995 Å at a sample–detector distance of 3 m. The images were normalized and azimuthally averaged to obtain the one-dimensional curves of intensity as a function of the scattering vector, $Q = \frac{4\pi}{\lambda}\sin(\theta/2)$, where θ is the scattering angle and λ is the X-ray wavelength. This was followed by averaging of curves from different frames and subtraction of the water background from the AzoTMA sample measurement to yield the final scattering curve presented here.

The predicted scattering patterna of the simulated aggregates were calculated using the explicit-solvent method of Hub and coworkers [38,39]. This method accounts explicitly for the hydration and the displacement of water by the micelles, which is in contrast to other methods using the Debye equation where such parameters would need to be fitted. Solely a scaling of the calculated curve is necessary to compare with the experimental data, since the intensity of the experimental data will scale with the concentration of micelles. Because our calculations are based on single micelles we cannot account for the interactions between particles, which cause certain distances between micelles to be preferred. These interactions give rise to interference patterns in the low Q regions of the scattering. In analytical modelling this can be accounted for in systems of low polydispersity by multiplication of the analytical *form factor* with an *apparent structure factor* that is independent of the form factor. We have similarly used an apparent structure factor simply to illustrate that the calculated scattering pattern can also fit the low Q data. The structure factor will not affect the scattering arising from the intramicellar structure as these length scales are much smaller than the length scales of intermicellar interactions.

3. Results and discussion

3.1. Characterization of trans-AzoTMA micelles at thermodynamic equilibrium

Fig. 2 shows snapshots of the structures the *trans*-AzoTMA micelles at different values of the aggregation number P, after preparation as

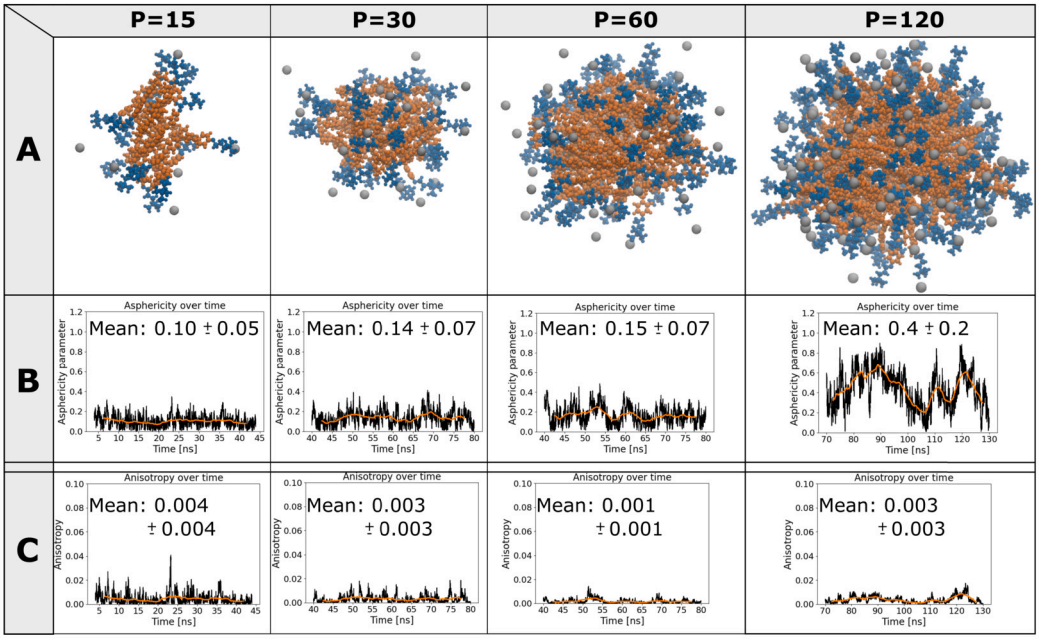

Fig. 2. The structure of the *trans*-AzoTMA aggregates formed by different numbers of molecules. Panel A shows a snapshot of the moieties taken from the simulations, with aggregation number indicated in the different columns. The ions located within 1 nm of the micellar surface have been included in the visualisation. Panel B and C shows the asphericity parameter and anisotropy, respectively, calculated over a certain time of the simulation with the running average over every 500 ps shown by the orange line. (For interpretation of the colous in the figure(s), the reader is referred to the web version of this article.)

described in section 2.4 and summarized in Table A.2. In all cases, the overall shape is qualitatively spheroidal. For a more quantitative measure of the micellar shape, the asphericity and relative shape anisotropy were evaluated over time for the different aggregates as shown in Panels B and C of Fig. 2. The calculated asphericity fluctuates between 0 and 0.4 nm^2 in the picosecond timescale for the smaller aggregates, with average values of 0.1 ± 0.05 nm^2, 0.14 ± 0.07 nm^2 and 0.15 ± 0.07 nm^2 for the aggregates of 15, 30 and 60 molecules respectively, while the $P = 120$ exhibits larger fluctuations with an average value of 0.4 ± 0.2 nm^2. These low values for the asphericity show that all smaller *trans*-AzoTMA micelles are on average very close to a spherical structure. On the contrary, the larger $P = 120$ aggregate tends towards more ellipsoidal structures. All the micelles also have a very low relative shape anisotropy, varying in all cases below 0.02, showing that the micelles are essentially spherical.

In an attempt to quantify the degree of order of the AzoTMA molecules in the micelles, histograms of the angle between the vector drawn from the AzoTMA headgroup to the end of the tailgroup of the molecule and the vector drawn from the headgroup of the molecules to the center of mass of the micelle was calculated for the different micellar aggregates. The found distributions are shown in Fig. B.14. The distribution of angles narrows and moves closer to 0°as the aggregation number increases; in particular the distribution becomes more defined and always below 90°when increasing from 30 to 60 molecules. The distribution does, however, have a tail going to 90°, showing that some molecules are indeed located parallel to the surface of the P = 120 micelle. Another measurement of micellar order is the radial distribution function (RDF) for each of the different moieties composing the AzoTMA molecule going from the center of the micelle (Fig. B.15). The RDFs broadly confirm that on average the molecules are oriented with the tail group towards the center and the headgroups facing outwards. However, the distributions are quite wide, especially for the hydrophobic part, so that we have a significant amount of the tailgroup distributing into the headgroup region.

Although micelles of different size may be present in the experimental samples, especially as transient species during initial aggregation, at specific thermodynamic conditions certain shapes are likely to be predominant over the others. In order to identify if this is the case also for *trans*-AzoTMA, we compared the aggregates at different P obtained from simulations with experimental SAXS data. The top left of Fig. 3 shows the experimental SAXS spectrum of AzoTMA from [30].

The right of Fig. 3 shows the comparison of scattering pattern calculated from the simulated micelles of different aggregation number with the experimental data. It is quite clear that the SAXS spectrum calculated from the $P = 120$ aggregate alone fits much better the experimental data than the other aggregates within the length scale resolution of the simulation, which corresponds to a Q-range going down to approximately 0.04 $Å^{-1}$. Thus, we can assume this to be an excellent model for the micelles found in the experimental sample. The calculated scattering pattern also describes the high Q scattering much better as compared to the analytical homogeneous core-shell models previously used for the same system [30]. This suggests that the packing disorder, as opposed to an ideal segregation between a *hydrophobic core* and a *hydrophilic shell* used in the analytical modelling, is a characteristic structural feature of the micelles.

In the absence of significant inter-particle interactions, we can normally use the intensity extrapolated at Q = 0 to determine the molecular weight of the individual aggregates and thereby the aggregation number if the density of the molecules is known. However, the AzoTMA micelles have a high charge density due to the positively charged headgroups, which results in strong inter-particle repulsion. This causes the particle scattering to be modulated by scattering interference between aggregates at the low Q values, so that the I(Q = 0) values cannot be accurately determined from the experimental data. Similarly, our calculations which are based on single micellar units cannot be expected to replicate the low Q data due to the lack of information about inter-particle distances. However, as discussed above, we do see significant differences in the structure and packing of micelles of difference aggregation number, so we can still see which micelles most accurately reproduce the intermediate and high Q SAXS data. The Hayter-Penfold structure factor, as used in the previous analytical modelling of the experimental data [30], was multiplied with the SAXS intensity calculated from the $P = 120$ simulation using Jscatter [48] and is shown as the

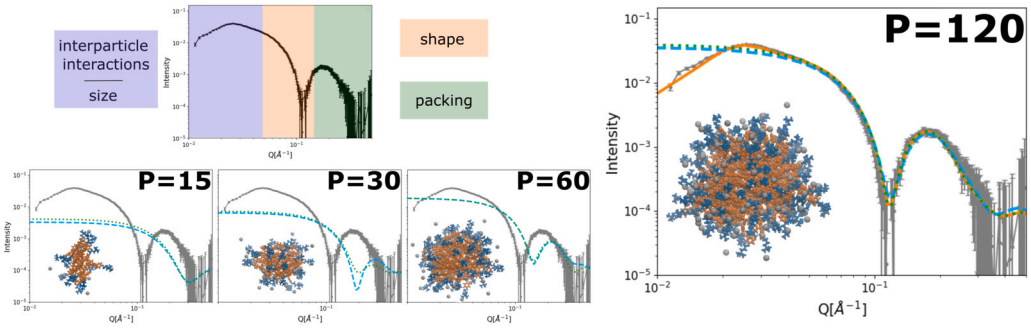

Fig. 3. Experimental SAXS data for *trans*-AzoTMA micelles in water solution (14.6 mM) as taken from [30] compared with the scattering pattern calculated from simulations of AzoTMA at different aggregation numbers P. Dashed and dotted blue and green lines represent the scattering patterns calculated from the respective structures (P = 15, 30, 60 and 120) at two different timepoints in the simulations. The full orange line for P = 120 represents the calculated data multiplied with the Hayter-Penfold structure factor to account for inter-particle repulsion. The top left of the figure illustrates the typical structural information one can extract from the different Q-ranges, where the Q-values are reciprocal to the real space dimensions.

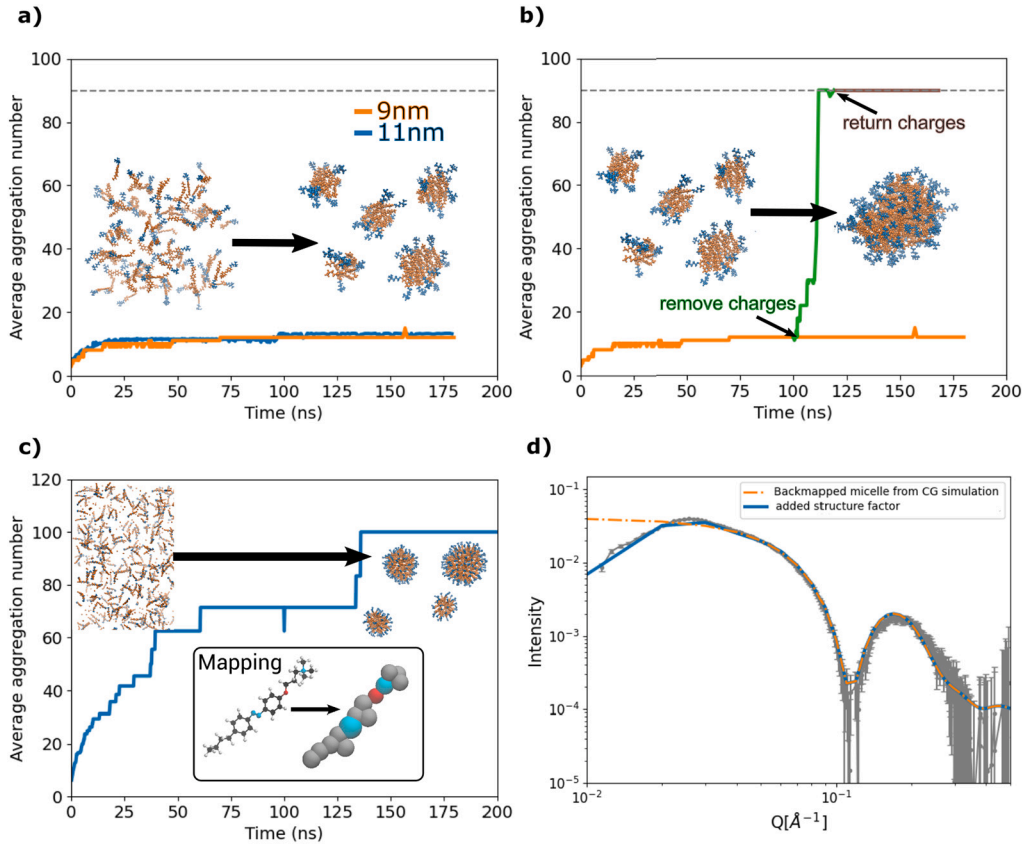

Fig. 4. a) Plot of the average aggregation number as a function of time from the starting point of randomly dispersed AzoTMA molecules in solution for two differently sized systems with the same concentration of molecules (90 and 234 molecules in 9 nm and 11 nm cubic boxes respectively). b) Plot of the average aggregation number as a function of time of aggregation of 90 molecules in a 9 nm cubic box with charges and where the headgroup and ion charges are removed and returned causing further aggregation of the initial clusters. c) Plot of the average aggregation number over time for a Hamiltonian hybrid particle-field molecular dynamics simulation of coarse-grained *trans*-AzoTMA, mapped as shown in the inset, starting from an randomly dispersed state of 500 surfactants. d) Scattering patterns calculated from a micelle of 118 molecules obtained in the simulation in c) which was backmapped to the all-atom representation without (orange dashed line) and with added structure factor (blue full line) compared with the experimental data (error bar plot in grey).

orange line in Fig. 3 to illustrate that it can also give a reasonable explanation of the low Q data when structure arising from inter-particle repulsion is taken into account. The structure factor will only affect the scattering at the low Q range (corresponding to real space distances of more than 20 nm) which is anyway inaccessible from our simulations, and is thus only added to the best fitting data of the accessible range for illustrative purposes.

3.2. Micellar kinetics of trans-AzoTMA in water

We simulated the aggregation of *trans*-AzoTMA starting from an initial configuration of randomly dispersed molecules in water. Fig. 4a shows the average aggregation number as a function of time, at a concentration of 205 mM. Simulations were repeated changing the total size of the system without changing the concentration, to rule out

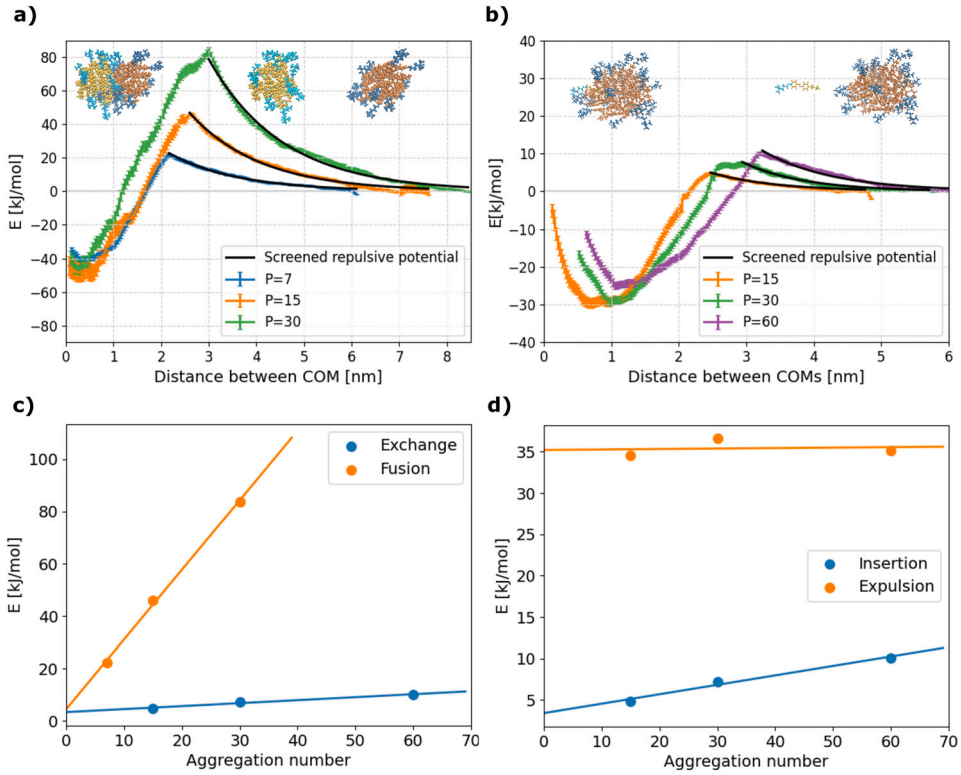

Fig. 5. a) The potential of mean force for fusion of micelles with aggregation number P. Legend refers to aggregation number before fusion. The right sides of the curves have been fitted to a screened repulsive potential. b) The potential of mean force of exchange of single molecule into micelles of different aggregation number P. Legend refers to aggregation number before insertion of molecule. The right sides of the curves have been fitted to a screened repulsive potential. c) The variation of the activation energy for fusion or exchange (insertion of one molecule) as a function of the aggregation number of the involved micelles, with linear fits to data. d) The activation energy for insertion or expulsion of a single molecule as a function of the aggregation number of the remaining micelle, with linear fits to data.

potential finite-size bias in the results. The aggregation into small aggregates is initially very fast, occurring within the first 20 ns. After this, there are few free monomers left in solution and big increases in the aggregation number depend on fusion of the smaller units. The aggregation number seems to stabilize at an average of 12 molecules after the first 100 ns. This is similar to what has been reported in molecular dynamics studies of other charged surfactants, [49,50], where their initial aggregation also occurs within the first 10-20 ns and then seemingly stops at aggregation numbers much lower than the expected ones. This is in stark contrast with uncharged and zwitterionic surfactants, where complete aggregation of all molecules was observed to happen within the first 50 ns [49,50]. It was also found for SDS that there was a large potential barrier for fusion of the initially aggregates [49]. Similarly here, we expect that an energy barrier of similar magnitude was preventing fusion of the small aggregates. By removing the net charge on the head-group and counter-ions, all 90 AzoTMA molecules that were simulated in the box aggregated into a single micellar unit within 15 ns, as shown in Fig. 4b. The formed micellar aggregate remained stable after returning the charges to the system. Coarse-grained molecular dynamics simulations with smoothed potentials such as Hamiltonian hybrid particle-field molecular dynamics [51,52] can be used to overcome the required kinetic activation, and to produce fully equilibrated micelles (Fig. 4c). Picking a $P = 118$ aggregate from a simulation of 500 coarse-grained AzoTMA molecules and backmapping it to the all-atom structure also yields a scattering pattern that fits well to the experimental data (see Fig. 4d). This computational experiment also shows that the nature of the kinetic barrier slowing down the aggregation process is enthalpic, and heavily influenced by the electrostatic repulsion among the charged head-groups.

The growth of fully formed micelles from small micellar clusters may occur according to two mechanisms: either by progressive depletion of smaller systems by single molecule exchange, or by direct fusion of two micelles. We performed different sets of umbrella sampling simulations to evaluate the energy barrier for these two processes, as reported in Fig. 5. The energy barriers for both the fusion and the insertion of single molecules are dominated by the repulsive potential arising from the interaction between the charged headgroups. This is evidenced by the fact that the right side of the potential energy curves in Fig. 5a and b all conform to a screened repulsive potential of the type that is deduced in Derjaguin-Landau-Verwey-Overbeek (DLVO) theory [53,54]. The effective Debye length (λ_D) found from fits of the curves to this type of potential is found to be around 1.5 nm for the approach of two micelles in the fusion event. This corresponds very well to the nominal concentration of the electrolytic surfactant. Working in the absence of a salt, we notice a slight increase in the values of λ_D with increasing the size of the micelles (1.45 ± 0.01 nm, 1.48 ± 0.01 nm and 1.56 ± 0.02 nm, for P = 7, 15, and 30, respectively). This can be rationalized in terms of a progressive decrease of freely mobile charges upon aggregation of the surfactants, with counter-ions also binding to the micellar surface.

After reaching the maximum energy, which occurs when the headgroup surfaces are touching in the case of fusion, the headgroup rearrange to surround the hydrophobic tailgroups, and the free energy drops until the newly fused micelle has reached the equilibrium density. As seen from Fig. B.16, fusion occurs as the large, exposed hydrophobic patches on these small aggregates come into close contact, thereby not requiring otherwise major reorganization of the molecules to keep the headgroups toward the solvent.

For fusion, as reported in Fig. 5a, the free energy barrier is very high even for the smallest aggregation number tested, with a barrier of 22.1 kJ/mol found for the smallest micelles of 7 *trans*-AzoTMA molecules. The fusion rate constant can be estimated from the free energy function up to the energy maximum as described by Kawada et al. [49] and

for the $P=7$ aggregates is found to be 3457.7 $M^{-1}s^{-1}$, so that for the system simulated here we would expect fusion events to occur on the millisecond timescale. The activation energy for fusion increases linearly with a slope of 2.7 kJ mol^{-1}/P with the size P of the micelles (Fig. 5c), making it increasingly difficult for fusion to occur. From the extrapolation of the trend in Fig. 5c, the fusion of two aggregates of 60 molecules to form the $P=120$ micelle compatible with the SAXS data would have an energy barrier of 162 kJ/mol. With such high energy barrier one would not expect fusion to be an important pathway in the equilibration of micelles of large aggregation numbers. Fusion of the very small aggregates, as in the case of 7 molecules, however, remains a likely mechanism in the initial pre-micellar cluster formation. Such events are indeed observed in the initial aggregation (Fig. 4); for example, the formation of the largest resultant micelle from this simulation is the result of fusion between a $P=7$ and a $P=8$ aggregate.

The obtained potential energy curves for the exchange process can be seen in Fig. 5b. The stabilization energy of the exchange process is measured as the global energy minimum; the energy increases again at very short distances due to the penetration of the charged AzoTMA headgroup into the hydrophobic core of the micelle. The activation energy for the insertion of one AzoTMA molecule (ranging from 5.9 ± 0.3 to 10.1 ± 0.4 kJ/mol) is significantly smaller than that for fusion of two aggregates, and as seen from Fig. 5c it depends only weakly on the aggregation number with a fitted slope of 0.11 kJ mol^{-1}/P. However, the exchange process consists of the expulsion from a micelle as well as the insertion of a unimer to a different micelle, so we need to consider both these processes. From Fig. 5d, we see that while the activation energy of expulsion (35 ± 1 kJ/mol) is much higher than that of insertion, it is still lower than that of most fusion/fission processes, and it shows essentially no dependence on the aggregation number. This means that expulsion remains a possibility regardless of the state of the system. Since the probability of an expulsion event will also depend on the number of AzoTMA molecules present rather than the number of micelles, expulsion events are expected to occur much more frequently as the micelles become larger.

Together, the results from the free energy calculations indicate that the main mechanism for equilibration after initial nucleation of the pre-micellar clusters is exchange of single molecules for the system of *trans*-AzoTMA in water. Weak variations with increasing P of the energy barriers for unimer in/out exchanges contrast with the marked increases of both the fusion and fission barriers. This suggests that the relative rate of fusion/fission processes as compared to unimer exchanges will rapidly vanish with increasing P. Altogether, one concludes that unimer exchanges are predominant in the equilibration of the largest micelles. In the case of growth kinetics, this therefore supports the kinetic theory of Aniansson and Wall [6] that the kinetics can be assumed to be step-wise for very large micelles. Importantly, however, in generalizing these results, one must consider that if the equilibrium aggregation number is very small, fusion would be expected to play a larger role in the growth processes. This is also in line with the calculations of Dormidontova [14] on polymer micelles showing that the barriers for fusion increase significantly as compared to unimer exchange with increasing size. The equilibrium aggregation number is therefore an important consideration when studying micellar kinetics as this will majorly affect the expected dominating mechanism.

3.3. Photo-isomerization of trans-AzoTMA micelles

The percentage of *cis*- molecules after photo-isomerization under constant UV light of dark adapted AzoTMA was previously found to be 84% [25]. Experimentally, it is accordingly possible to explore a broad range of *cis/trans* conversion ratio going from the dark-adapted state to the UV (photo)stationary state. Therefore, we performed a range of simulations where different percentages of randomly chosen *trans*-AzoTMA surfactants in the equilibrated $P=120$ micelle in water were converted to *cis*-AzoTMA using the switching potential as described in section 2.5. The structures immediately following the isomerization events can be seen in Fig. 6.

Splitting of the micelle occurs within the first 100 ns of relaxation when isomerizing more than 68% of the molecules. For the 68% isomerization, the $P=120$ micelle has not completely undergone fission within the 100 ns, but shows an elongated structure that split into two micelles within the next 30 ns. The higher isomerization percentage is imposed, the faster the splitting occurs, as it can also be seen in Fig. 7b. The fission events follow gradual elongation of the micelles. In all these cases, the $P=120$ aggregate splits into two aggregates, not necessarily similar in size; from Fig. 7b and c we see that for the systems where more that 84% of the molecules were switched to the *cis*-isomer we gain two aggregates of very different anisotropy and asphericity parameters. From the asphericity, we see from Fig. 7c that one aggregate is above one suggesting an elongated particle and one is close to zero and therefore a quite spherical particle. We could not see any significant difference in the relative amounts of *cis*- and *trans*-isomers between the micelles that have undergone fission. Thus the different "packing parameters" or potential segregation between the two different isomers does not seem to play any role in the fission process or the resultant structure of the micelles. It is the overall reduction in the hydrophobicity of the isomer mix that favors smaller aggregates to re-balance the forces from the interface and repulsion between the headgroups, and the fast out-of-equilibrium transition causes the formation of quite polydisperse resultant structures. As discussed by Dormidontova, although fission into equal aggregates may be more thermodynamically favorable, fission with expulsion of a smaller micelle will have a higher rate constant and is therefore kinetically favored [14].

None of the micelles resulting from isomerization of the $P=120$ micelle fit well with the experimental data. Fig. 8a shows two examples, where we can see that the resulting larger micelle from the 76% isomerization is too small whereas the 52% isomerization gives a SAXS pattern that is very similar to that of the original *trans*-micelle, which is slightly too large. A possible explanation for that is that the very rapid fission process observed in the simulations is likely followed by a longer period of re-equilibration and regrowth of the split micelles via molecular exchange. This bears similarities to experimental observations of block polymer micelles undergoing cylinder-to-sphere [55] or sphere-to-sphere transitions where the experimental data clearly show a fission process into sub-micelles followed by molecular exchange process that leads to final equilibrium structure.

Interestingly, 68% isomerization of the smaller $P=90$ *trans*-AzoTMA micelle does not undergo splitting, yielding a mixed *cis-trans*-micelle that fits very well the experimental SAXS data, as can be seen in Fig. 8b. From the RDF reported in Fig. B.17a, we can deduce that the overall structure of the micelle is not so different from the original all-*trans*-aggregate. Many of the *cis*-molecules present align in a more skewed orientation with respect to the direction from the center of mass to the surface of the micelle, to keep the tail groups close to the original positions in the all-*trans*-aggregate. The shape of the micelle remains spheroidal, close to spherical, as indicated by the asphericity parameter and anisotropy as shown in Fig. B.17b and c, while the average radius of gyration is actually slightly larger (2.0 nm) compared to the original *trans*-micelle (1.9 nm), suggesting a small decrease in the density of the molecules.

3.4. Mechanisms for micellar dissolution upon photo-isomerization

At experimental conditions, we can imagine the changes in aggregation number observed during the isomerization event to be the result of one of two different processes. Firstly, it can be thought to occur through fission, as observed for our system, followed by re-equilibration of the new micelles by unimer exchange. This is in many ways similar to the micelle formation mechanism suggested by Pool and Bolhuis based on their molecular simulations [15] and the mechanism for out-of-equilibrium kinetics suggested by Dormidontova [14]. Secondly, the

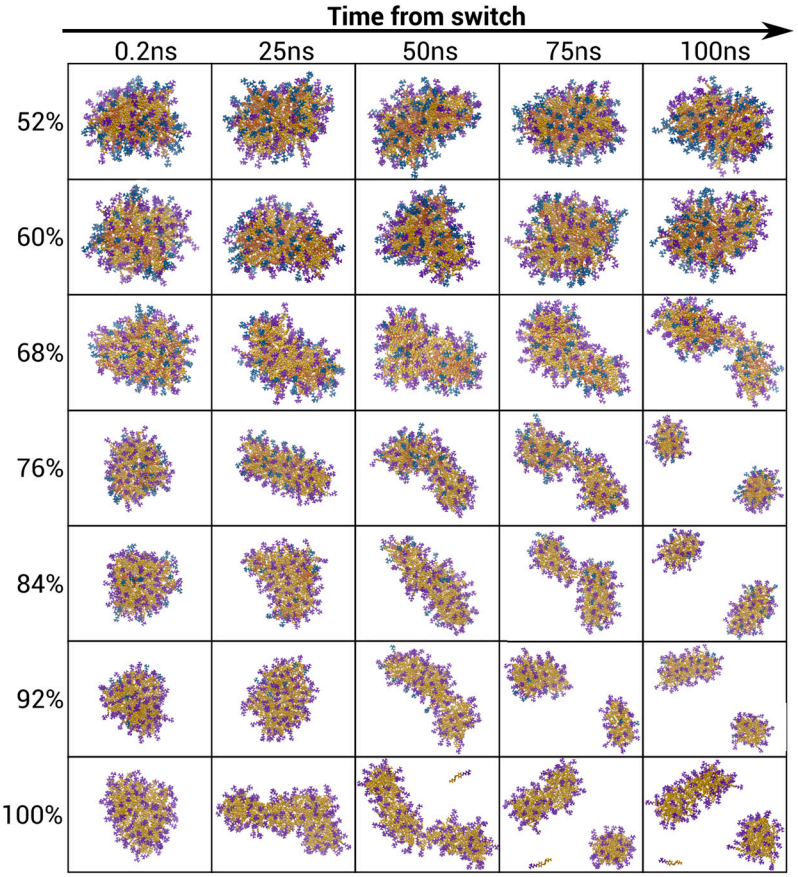

Fig. 6. The time evolution of the P = 120 aggregate after different % of *trans*-AzoTMA molecules were switched to the *cis*-configuration.

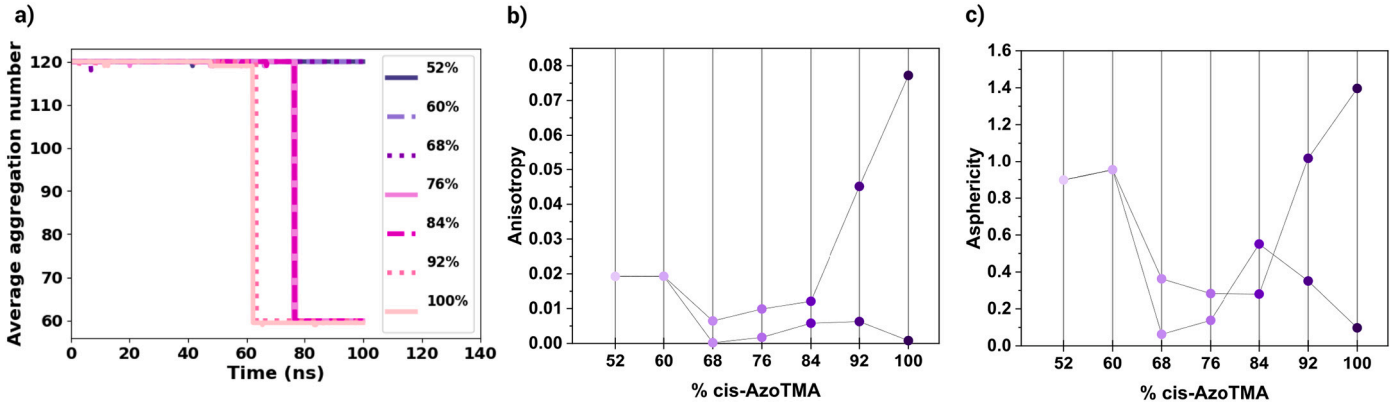

Fig. 7. a) The average aggregation number over the time following the isomerization event for different degrees of isomerization of the P = 120 aggregate. b) and c) display the anisotropy and asphericity parameter, respectively, calculated for the aggregates formed 100 ns after isomerization of different percentages of the AzoTMA-molecules to the *cis*-configuration.

isomerization might be followed by the dissolution of micelles through release of the less hydrophobic *cis*-unimer to the solution until the equilibrium aggregation number is reached for each micelle. In simulations the molecules are all instantaneously isomerized to the *cis*-state, whereas at experimental conditions the photo-illumination will last for a certain time and thus the number of molecules that are isomerized will be gradually increasing over time. In the simulations, or potentially in the conditions of a very short and intense laser pulse, the system will be pushed to a high energy state very fast without any time to equilibrate in the process. In the case of a gradual increase in the amount of *cis*-isomers during light illumination, however, the micelles could have time to equilibrate during the isomerization event. These two different scenarios could therefore yield very different kinetics.

One possible way to promote the second mechanism, where we have release of unimers, is to increase the hydrophilic/lipophilic balance of the surfactants, thus significantly raising the CMC. One method for tuning the CMC, also used by Lund et al. in their study [30], is by having a percentage of a chaotropic agent such as DMF in the aqueous solution. Fig. B.18 depicts simulations of *trans*-AzoTMA molecules aggregating from an initial random distribution in solutions of different volume fraction of DMF. In solutions of 50% of DMF, the AzoTMA molecules do not show significant aggregation - during MD runs we could only observe transient formation of aggregates up to 5 molecules, which anyway dissolve within few nanoseconds. To fully conclude that no aggregation occurs in 50% DMF, we also re-solvated the aggregates found from the control simulation in pure water in a 50% DMF solu-

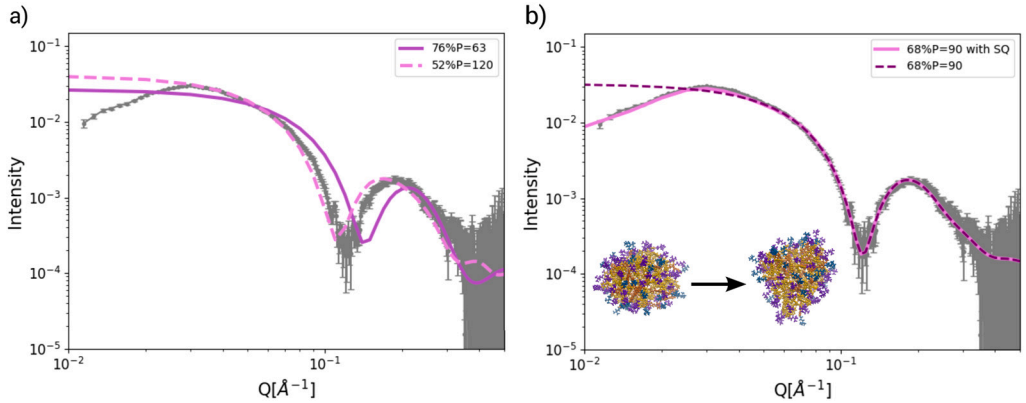

Fig. 8. a) SAXS data from AzoTMA micelles exposed to UV in water solution (14.6 mM) as taken from [30] compared with the scattering calculated from simulations of a) a P = 63 AzoTMA micelle where 76% of the molecules were isomerized to the *cis*-state (full line) and a P = 120 micelle with 52% isomerized (dashed line), and b) of a P = 90 AzoTMA micelle where 68% were isomerized to the *cis*-state and simulated for 100 ns.

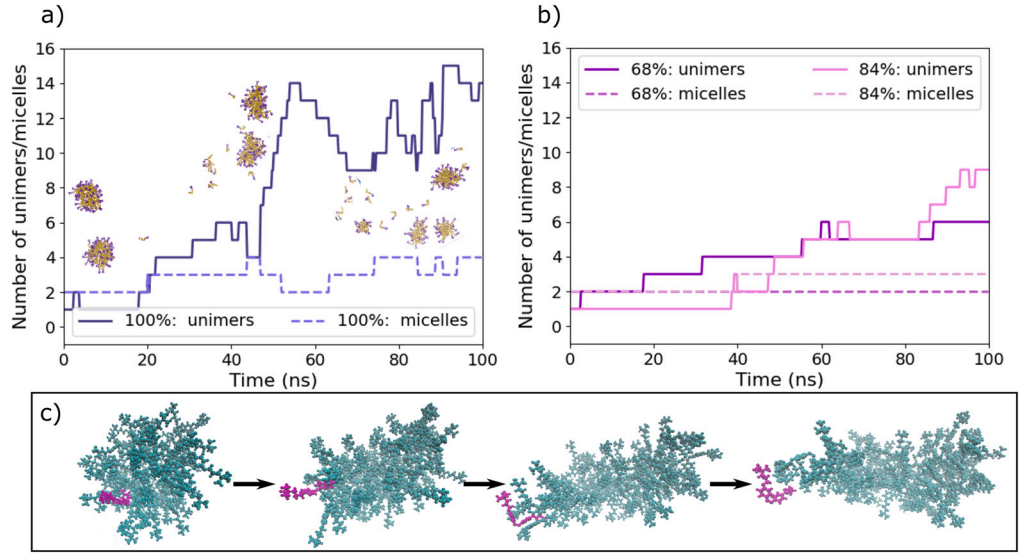

Fig. 9. a) The time evolution of the number of unimers and micelles in solution after *trans-cis* isomerization of the two aggregates ($P \approx 60$) of AzoTMA in 30% DMF. The dark blue, full line shows the number of free unimers, while the lighter blue, dashed line shows the number of micelles. b) The time evolution of the number of unimers and micelles after *trans-cis* isomerization of 68% and 84% of the two aggregates ($P \approx 60$) of AzoTMA in 30% DMF. The full lines show the number of free unimers, while the dashed lines show the number of micelles. c) The process of elongation of a micelle as seen in the simulation after the isomerization of 100% of molecules in AzoTMA aggregates dissolved in the 30% DMF solution. The elongation leads to monomer release at the stretched ends of the aggregate.

tion at the point indicated by the arrow in Fig. B.18, finding that the aggregates dissolved within 100 ns. The 30% DMF solution shows aggregation resulting in only a few very small stable aggregates and some free AzoTMA molecules. The reduced kinetic stability is confirmed from the occasional expulsion or intake of single molecules into the aggregates observed within the simulation times. To test the stability of the fully formed micelles, the $P = 120$ micelle was then re-solvated into the 30% DMF solution, mimicking an abrupt change in solvent. During a 275 ns-long simulation, the micelle quickly became more elongated until it finally split into two practically equally sized aggregates of 61 and 59 molecules (Fig. B.18b) after 125 ns, after which these aggregates remain for the next 150 ns. This further supports the reduced size of the *trans*-AzoTMA aggregates in the 30% DMF solution, caused by the reduction of the interfacial tension between the exposed hydrophobic parts of the micelle and the solvent. The reduced interfacial tension causes an increase in micellar shape fluctuations which increases the probability of "weak zones" where the micelle can fragment, as also observed by Maillet et al. [17].

Photoisomerization of the all-*trans*-AzoTMA in this 30% DMF solution gives quite drastic changes in the aggregation. The two micelles present in solution before the switch (taken from the simulation in Fig. B.18b at 200 ns) quite quickly start to split, as seen from the increase in micelles from two to three in Fig. 9a. The rupture of the micelle is accompanied by a large release of free unimers in solution, as seen from the large increase in the number of unimers from Fig. 9a. Specifically, the micelles become more elongated following the isomerization event and monomer release happens at the ends of these elongated aggregates, as illustrated in Fig. 9c. Interestingly, we observe that only the *cis*-isomers are released from the micelles when only a percentage of the molecules are isomerized (Fig. 9b). This is in agreement with the less hydrophobic character of the *cis*-conformation, in which a neat electrostatic dipole transversal to the N=N bond is present. Most of the monomers that are released into solution remain as unimers, only forming transient dimers or trimers. In the simulations of 68% photoisomerization in the 30% DMF, we also only observe unimer exchange of *cis*-AzoTMA and no fission/fusion (Fig. 9b).

The destabilization and increase of the concentration of free surfactants after isomerization in the DMF solution gives evidence that monomer release plays an important part in the mechanism of the *trans*-to-*cis* induced morphological changes that occur in the AzoTMA systems. However, since fission is observed both for the water systems that are far from the CMC and in the case of 100% isomerization in

30% DMF, it seems that fission can be an important route for equilibration for systems that have been photo-illuminated to yield a very fast out-of-equilibrium transition, a condition experimentally accessible only for surfactants with a very high quantum yield. For lower isomerization percentages in 30% DMF, we only observe release of unimers. This seems the more likely scenario for systems that convert intrinsically in a longer time-scale, or that are under conditions giving slow isomerization rates.

4. Conclusions

In this study we have elucidated different mechanisms for micellar kinetics in a photoresponsive AzoTMA surfactant system. Using surfactants with an azobenzene light-sensitive group is particularly relevant due to its popularity, which stems from the ease with which it can be incorporated into different chemical architectures and the stable and simple photochemistry [36]. AzoTMA has specifically been optimized to give a large shift in the value of the CMC upon photo-illumination [24], making it a good candidate for studying micellar aggregation and dissolution. The growth kinetics from an initially random state starts by the nucleation and formation of small, pre-micellar aggregates. As the aggregates become bigger, the fusion of two aggregates becomes increasingly more unlikely due to the high electrostatic repulsion between the clusters. Thus, the micellar kinetics becomes increasingly dominated by exchange kinetics rather than fusion as the exchange has both a lower energy barrier and have higher probability in numbers. Since the final validated aggregation number is at around 120 molecules, almost all of the growth must occur via exchange of unimers as the fusion of aggregates above 30 molecules is not possible. This is in line with the classical model of Aniansson and Wall [6] where relaxation is assumed to be dominated by unimer exchange. Fusion, on the other hand, is not found to be an important growth mechanism for the AzoTMA micelles unless the system is very far from equilibrium where micelles are small ($\approx 5\%$ of the final aggregation number), which is in line with the previous results of Dormidontova [14].

In the case of a disruption of the equilibrates micelle by an isomerization event, however, two different mechanisms were identified. In the case of a rapid shift into a state far from equilibrium, the micelles relax via both fission and release of unimers. This resembles the autocatalytic replication mechanism suggested by Pool and Bolhuis [15] as well as the fusion/fission + unimer exchange mechanism suggested by Dormidontova [14] where fission is found to be important for efficient re-equilibration of micelles under conditions where the equilibrium aggregation number has been decreased. When the shift from equilibrium is not as dramatic, as imagined in many experimental conditions where the isomerization will occur gradually over longer stretches of time, the micelles can relax through unimer release solely. This could help explain how some kinetic phenomena are mainly observed through molecular dynamics simulations, where the conditions are fully controlled in contrast to the lab experiments.

Fission was observed in different situations, that schematically resulted from a fast destabilization of the micelle producing out-of-equilibrium distributions and/or orientations of the molecules (via sudden *trans*- to *cis*- conversion, or DMF addition). Combined with a high Coulombic repulsion, a transient elongation of the destabilized clusters of surfactants relaxed by splitting into two fragments. This pathway was followed despite the high energy barrier for fission of the near-equilibrium assemblies. Interestingly, the time scale (100 ns) of triggered fission was of the order of magnitude of the formation time of micellar clusters, but much shorter than exchanges of the ionized unimers and micelle fusion events. This shows that the initial fast relaxation from the light-induced out-of-equilibrium state may follow a significantly different pathway than near-equilibrium kinetics, based on unimer exchange.

This study has given insight into the question of micelle kinetics under different out-of-equilibrium conditions. These conditions are not easily studied in the laboratory, thus molecular dynamics can provide details that are not obtainable with other available methods, including identification of different mechanistic pathways as well as calculation of thermodynamic parameters. Obtaining free energy values for exchange and fusion/fission from experimental measurements is difficult, thus computational techniques are very important in the study of micelle kinetics [56]. Other molecular dynamics studies have successfully studied the micelle kinetics of various surfactant systems [15,19,57–61], and the relevance of this technique to study mechanistic pathways in colloidal systems is continuously increasing with the improvements in computational efficiency and techniques [10]. The use of a photosensitive surfactant allowed us to study realistically relevant out-of-equilibrium conditions. Consideration of the micelle kinetics is important when optimizing the surfactant systems for a specific application [5,62]. The kinetics of photosensitive surfactants are of high interest due to their broad range of self-assembly tunability and their potential applications in technologies such as drug delivery systems, catalysis systems, diagnostics, and biosensors [37]. While photoresponsive surfactants have been investigated computationally in other contexts [32–35,63], this paper provides, to the authors knowledge, the first computational study that focuses on the micelle kinetics and mechanistic pathways of assembly and dissolution in these systems. We have also illustrated how this can be combined with experimental SAXS measurements to validate the micellar structures and ensure that we are investigating a system that is close to the experimental system.

The work presented here provides a basis for further investigations of how this and similar photoresponsive system will act in relation to their various applications. This includes investigating optimal kinetic conditions for controlled uptake/release of solute where investigations of the micelle properties have already been done for some conventional surfactant systems [64,65] and the kinetics in the presence of a external surface where photoresponsive surfactants have the potential to create photocontrollable foams and emulsions. Herdes et al. have already started investigating the interfacial behavior of photoactive surfactants computationally using a coarse-grained model [63]. Photoresponsive surfactant is also very relevant in mixture with other self-assembling molecules such as phospholipids [27], polymers [66–68] and DNA [69,70], which are even more complex to extract molecular detail and kinetic mechanisms from due to the range of structures and interactions that can occur in the systems, thus making it even more important to investigate the specific pathways.

Abbreviations

AzoTMA, 4-butyl-4'-(3-trimethylammoniumpropoxy)-phenylazobenzene; CMC, critical micellar concentration; DMF, dimethylformamide; MD, molecular dynamics; RDF, radial distribution functions; SAXS, small angle X-ray scattering.

CRediT authorship contribution statement

All authors contributed to writing, reviews and revision.

V.A. Bjørnestad: Conceptualization, Methodology, Software, Investigation, Formal analysis, Visualization, Writing – Original Draft; **X. Li:** Methodology, Software, Investigation; **C. Tribet:** Investigation; **R. Lund:** Conceptualization, Supervision, Funding; **M. Cascella:** Conceptualization, Supervision, Methodology, Funding.

Declaration of competing interest

The authors declare that they have no known competing financial interests or personal relationships that could have appeared to influence the work reported in this paper.

Data availability

The simulation data is freely and openly available at the GitHub repository https://github.com/Cascella-Group-UiO/Publications.

Acknowledgement

The authors acknowledge the support of the Norwegian Research Council through the CoE Hylleraas Centre for Quantum Molecular Sciences (Grant No. 262695) and NANO2021 (Grant No. 315666, RL) and the Norwegian Supercomputing Program (NOTUR) (Grant No. NN4654K). MC acknowledges funding by the Deutsche Forschungsgemeinschaft (DFG) within the project B5 of the TRR-146 (Project No. 233630050) and DFG Mercator Fellowship program. CT acknowledges support from the French Agence Nationale de la Recherche ANR Fliposomes (ANR-20-CE06-0007). The authors thank ESRF for the provision of beam time SC-4184.

Appendix A. Computational protocols and setup

A.1. Initial aggregation from dispersed state

AzoTMA molecules were placed in a random configuration into the empty simulation box using the GROMACS program `insert-molecules`. The box was then solvated with TIP4P [40] water using the GROMACS program `solvate` and Bromide ions were added to charge neutralize the system using the GROMACS program `genion`. The fully assembled system was then relaxed by steepest descent minimization (< 1000.0 kJ mol^{-1} nm^{-1}). This was followed by equilibration of the system by performing a position restrained simulation of 200 ps in the NVT ensemble to stabilize the temperature at 298 K with the CSVR thermostat followed by a 200 ps simulation in the NPT ensemble to stabilize the pressure to 1 bar with Parrinello-Rahman barostat. The production simulation were started as a continuation of the NPT-simulations without the position restraints on AzoTMA molecules. The particle mesh Ewald (PME) was used to calculate the long-range electrostatics, while short-range nonbonded interactions were cut off at 1.0 nm, and periodic boundary conditions applied in all directions. A table listing the system configurations and simulation times for the different simulations is given below.

Individual micelles could be the extracted from the simulation using a python script that identified aggregates of AzoTMA molecules and wrote out the corresponding coordinates to a separate file.

For the simulation where the charges on the AzoTMA molecules were removed, the configuration of Simulation 1 in Table A.1 at 100 ns was used. The topology was changed so that the charges on the Br^- ions were removed and the charges on the AzoTMA trimethylammonium atoms were changed to give a dipolar charge group. The simulation without charged molecules was run as a continuation from the 100 ns simulation for 20 ns. The original AzoTMA topology was then reintroduced and the simulation was continued for another 50 ns.

A.2. Simulations of assembled micelles

For the simulations of AzoTMA micelles at different aggregation numbers given in Fig. 2, micelles of the specific aggregation numbers were extracted from other simulations; an overview of where the different micelles were taken from can be seen in Table A.2. The micellar structure was re-solvated in the new simulation box using the GROMACS program `solvate`, followed by charge neutralization the system of the system again with Br^- ions using the GROMACS program `genion`. The assembled system then went through minimization and equilibration in the exact same way as described in section A.1 before starting the production runs. A table listing the system configurations and simulation times for the different simulations is given below.

The micelles arising from simulation of the fusion event as described in Section 2.4 stabilized quickly, albeit with the necessary equilibration time needed increasing with the size of the aggregate, as can be seen from Fig. A.10.

A.3. Umbrella sampling simulations

The micelles from Section A.2 we used to create the starting configurations for the umbrella sampling simulations. For the sampling of the fusion/fission event where the reaction coordinate is the distance between the centers of mass of the two approaching micelles, duplicates of the micelle used (aggregation number of 7, 15 or 30) were placed in the center of a cubic box. The micelles were first placed at the maximal distance away from the center of the box in the z-direction and then iteratively moved closer by 0.05 nm up to 2 nm distance and then 0.1 nm to generate each window for the umbrella sampling, giving a difference of 0.1 nm in the center of mass difference between windows in the range 0 to 2 nm, and 0.2 nm after. The configuration underwent energy minimization after each displacement, and the following energy minimized configuration was used to generate the next window. The cubic boxes were then filled with water and the neutralizing ions using the same procedure of `solvate` and `genion` in GROMACS as described in the previous sections. This was then followed by energy minimization and position restrained NVT and NPT equilibration as also described in the previous section. In the case of fusion between a single molecule with a micelle fusion, the same procedure for generating starting configuration as above was used with the TMA-group facing away from the COM of the micelle in the initial configuration, and this was followed by the same minimization and equilibration procedure as above. The spacing between windows in these cases were 0.1 nm in the full range of distances. The system configurations for the different umbrella simulations are given in Table A.3.

The production umbrella sampling simulations were then run with an harmonic potential and force constant of 1000 kJ mol^{-1} nm^{-2} for 10 ns whereby the first ns was discarded for each window generated. Analysis of the results were performed using the weighted histogram analysis method (WHAM) as implemented in GROMACS [46]. Overlap of the resulting histogram was checked, and if any gap was observed additional simulations at the distance between the non-overlapping

Table A.1
System configurations for simulations of the initial aggregation from a dispersed state.

Simulation name	Number of AzoTMA molecules/Br ions	Sides of cubic box(nm)	Number of water molecules	Number of DMF molecules	Simulation time (ns)
Simulation 1: Pure water	90	9.0	22313	0	182
Simulation 2: Pure water	234	11.0	39123	0	188
Simulation 3: 17% DMF	15	9.0	20998	963	200
Simulation 4: 30% DMF	15	9.0	15992	1701	300
Simulation 5: 50% DMF	15	9.0	11636	2835	300

Table A.2
System configurations of assembled micellar structures for equilibration.

Simulation name	Micelle origin	Sides of cubic box (nm)	Number of AzoTMA molecules/Br ions	Number of water molecules	Number of DMF molecules	Simulation time (ns)
P15	Simulation 1 of Table A.1	10.0	15	32984	0	64
P30	Fusion simulation of 2 micelles of P = 15	11.0	30	43677	0	80
P60	Fusion simulation of 2 micelles of P = 30	12.0	60	56176	0	80
P120	Fusion simulation of 2 micelles of P = 60	15.0	120	109773	0	130
DMF30P120	Simulation P120	15.0	120	72842	7695	275

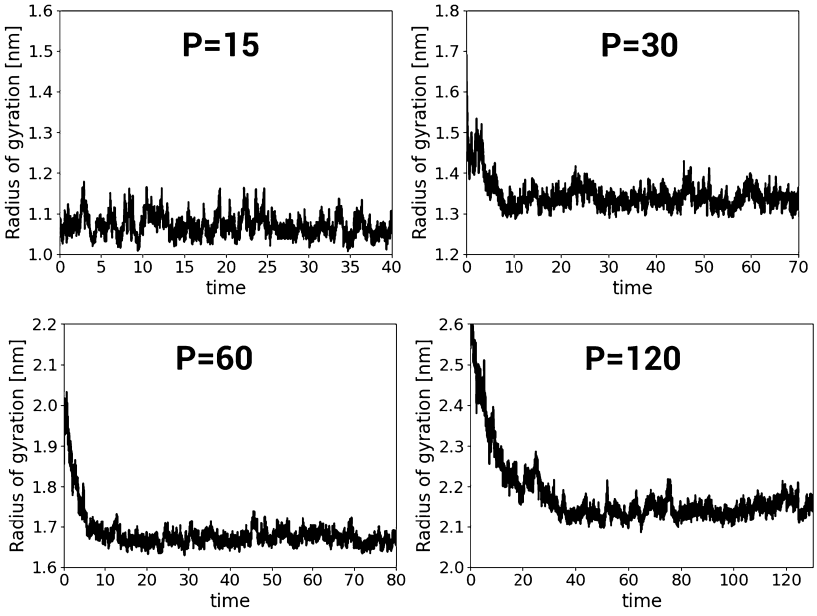

Fig. A.10. Radius of gyration over time. For P = 30, 60 and 120 the radius of gyration is higher at the start of the simulation as the micelles are fusing together.

Table A.3
System configurations for umbrella sampling simulations.

Simulation name	Micelle origin	Sides of cubic box (nm)	Number of AzoTMA molecules/Br ions	Number of water molecules
2xP7	Simulation 1 in Table A.1	13.0	14	72889
2xP15	Simulation 1 in Table A.1	15.0	30	111781
2xP30	Simulation P30 in Table A.2	17.0	60	162356
P15+1	Simulation 1 in Table A.2	10.0	16	32962
P30+1	Simulation P30 in Table A.2	12.0	31	56883
P60+1	Simulation P60 in Table A.2	14.0	61	88807

windows were performed to correct this. The histograms for each of the umbrella simulations can be seen in Fig. A.11 which along with the smooth function for the free energy which was obtained confirms the overlap of the histograms. The statistical error was calculated using the bootstrapping technique with 100 bootstraps (Fig. A.12).

A.4. Photo-isomerization simulations

After applying the modified potential for 20 ps, production MDs simulations were run according to the same procedure as described in the Methods section for the systems described in Table A.4. For the simulations in pure water, the end configuration of simulation P120 of Table A.2 was used whereas for the ones with DMF the end configuration of simulation DMF30P120 of Table A.2 was used.

Appendix B. Additional simulation results

B.1. Structural characterization of micelles of different aggregation number

See Figs. B.14 and B.15.

B.2. Aggregation of randomly dispersed trans-AzoTMA in water

See Fig. B.16.

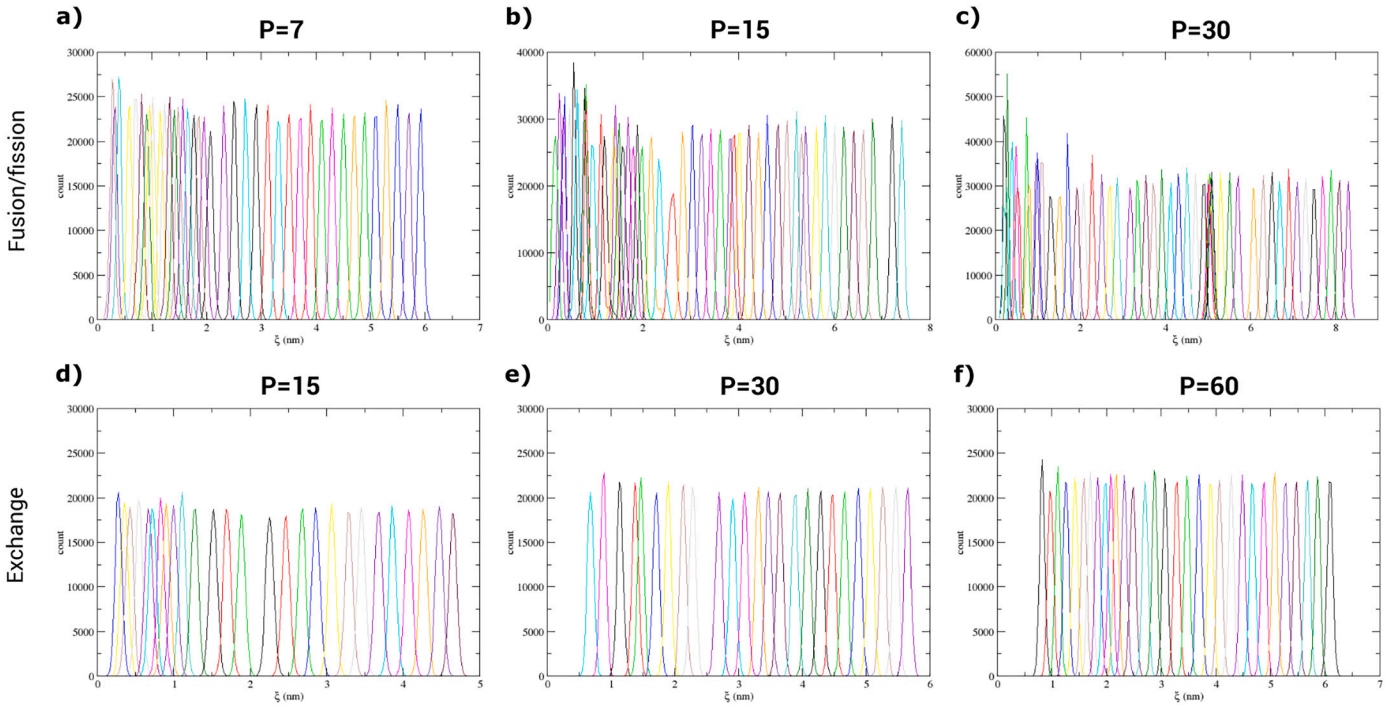

Fig. A.11. Histograms obtained from the umbrella sampling windows of the fusion/fission event for micelles of aggregation number, P, a) 7, b) 15, and c) 30, and for the single molecule exchange for the micelles of P+1 aggregation number for P equal to d) 15, e) 30 and f) 60.

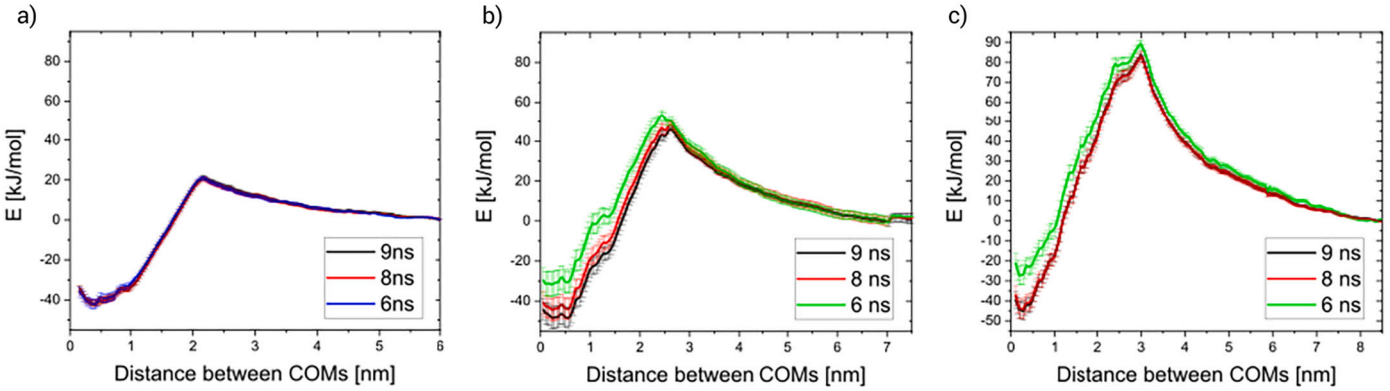

Fig. A.12. Comparison of the curves obtained for the potential of mean force for fusion for different simulation times for the a) 2xP7, b) 2xP15 and c) 2xP30 umbrella sampling simulations.

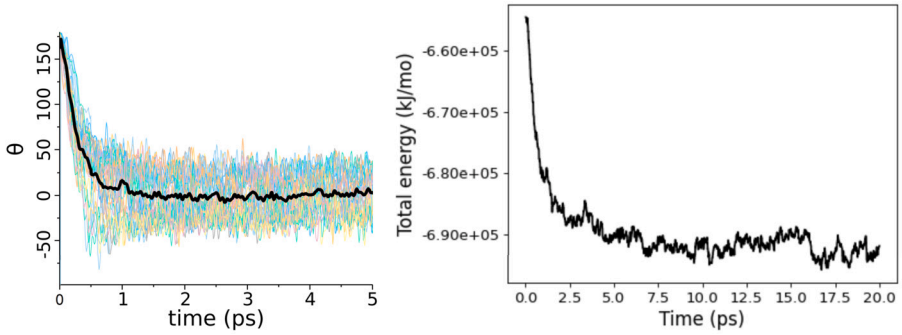

Fig. A.13. a) The dihedral angle of the azo-group as a function of time after the modified potential has been switched on. Colored curves represent individual dihedrals while the black curve is the average at each timepoint. b) Total energy of the system as a function of time after the modified potential has been switched on.

Table A.4
System configurations of trans-to-cis switching simulation.

Isomerization percentage	Sides of cubic box after NPT equilibration (nm)	Number of trans-AzoTMA	Number of cis-AzoTMA	Number of water molecules	Number of DMF molecules	Simulation time (ns)
100	15	0	120	109773	0	100
92	15	10	110	109773	0	100
84	15	19	101	109773	0	100
76	15	29	91	109773	0	100
68	15	38	82	109773	0	130
60	15	48	72	109773	0	100
52	15	58	62	109773	0	100
100	15	0	120	72842	7695	100
84	15	19	101	72842	7695	100
68	15	38	82	72842	7695	100

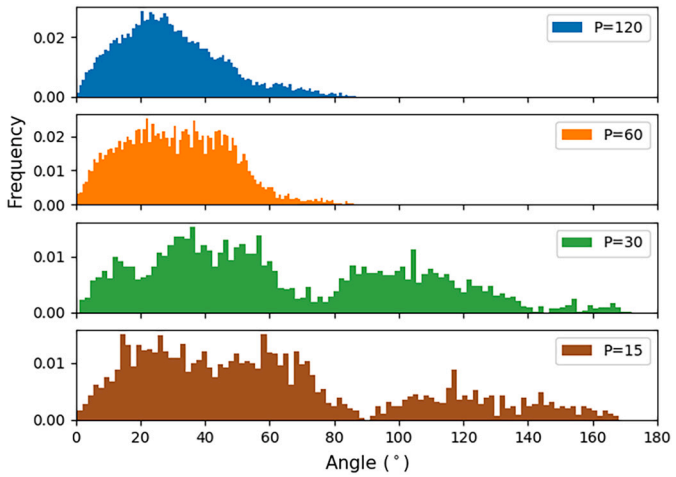

Fig. B.14. Histogram of the order parameter taken over all molecules in aggregates of AzoTMA of different size over 1 ns.

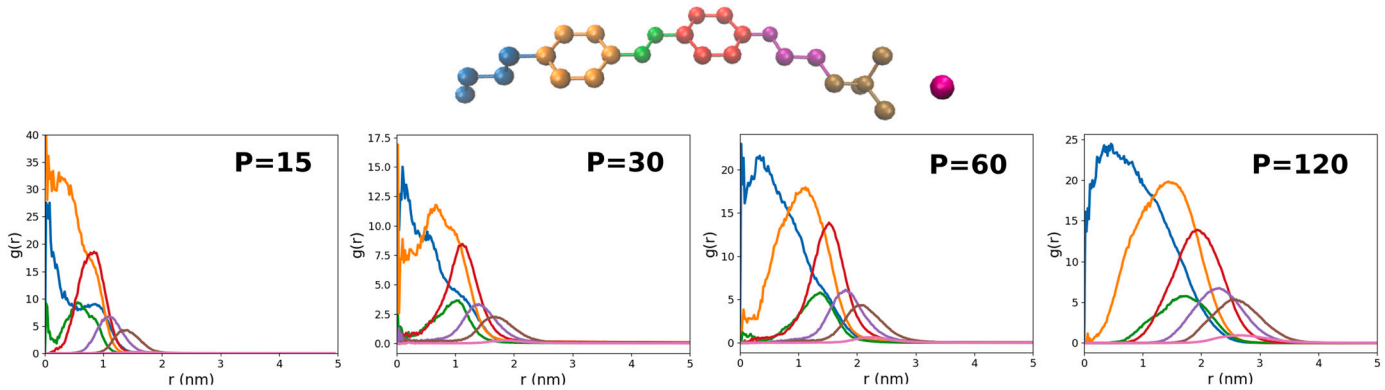

Fig. B.15. Radial distribution function from the center of mass of the micelles of the different group of the molecule as indicated by the figure for the differently sized micelles.

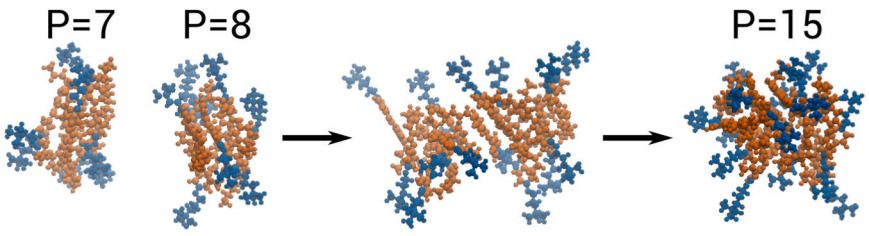

Fig. B.16. Snapshots from the fusion of two clusters of 7 and 8 molecules into a cluster of 15 molecules as observed in the aggregation simulation.

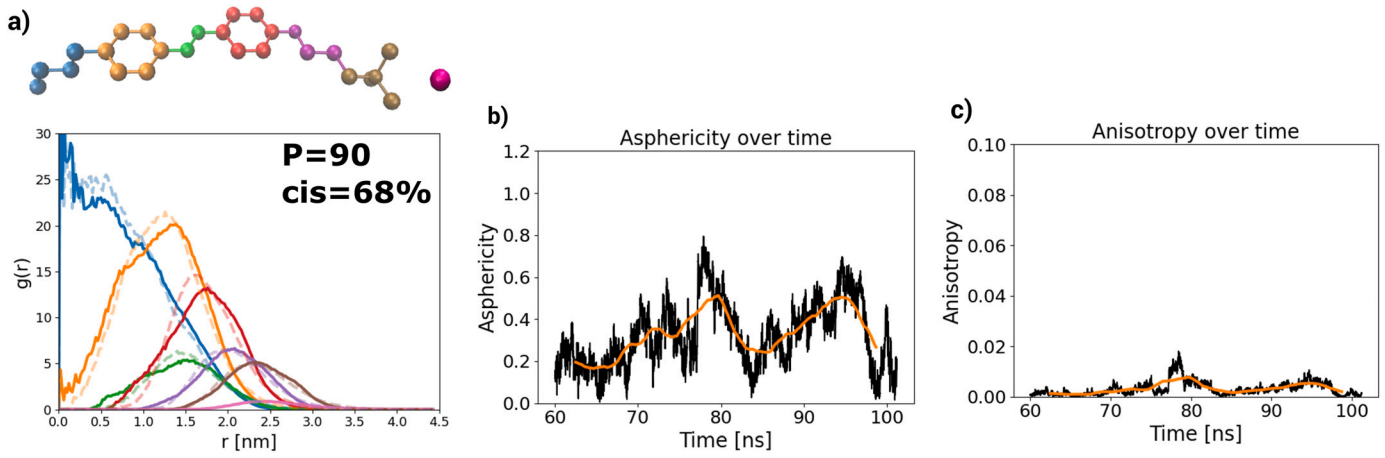

Fig. B.17. Structure of the P = 90 micelle with 68% isomerization of molecules. a) Radial distribution function from the center of mass of the micelles of the different group of the molecule as indicated by the figure for the micelle (full line). Dotted, transparent line shows the full-*trans*- P = 90 micelle for comparison. b) The asphericity parameter and c) anisotropy of the isomerized P = 90 micelle calculated over a certain time of the simulation.

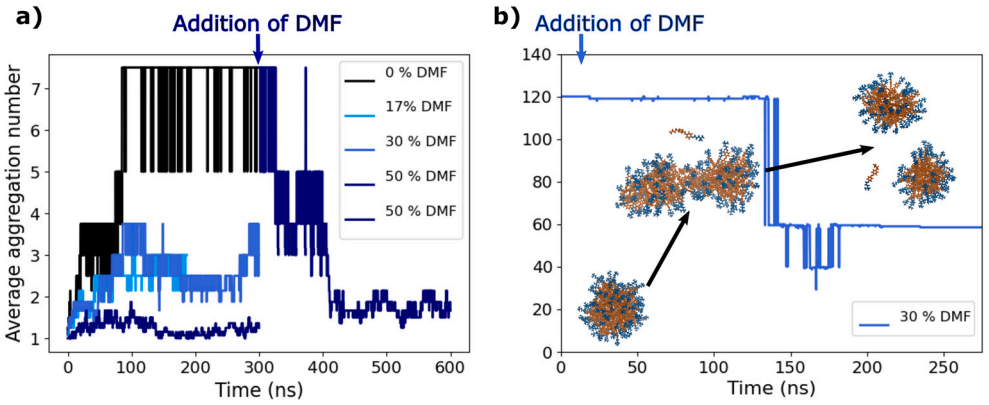

Fig. B.18. a) Plot of the average aggregation number as a function of time from the starting point of randomly dispersed AzoTMA molecules in solution for systems with 15 AzoTMA molecules with different volume fractions of DMF in the solvent. DMF was also added to the control with no DMF after 300 ns.b) Plot of the average aggregation number as a function of time as 30% DMF is added to a micelle of aggregation number of P = 120. The micelle first elongates before fissioning into two micelles.

B.3. RDF of P = 90 micelle with 68% isomerization of molecules

See Fig. B.17.

B.4. Effects of DMF on aggregation of trans-AzoTMA

See Fig. B.18.

B.5. Calculations of asphericity and anisotropy

The asphericity parameter b is calculated from the principle moments, λ, as:

$$b = \lambda_z^2 - \frac{\left(\lambda_x^2 + \lambda_y^2\right)}{2} \tag{B.1}$$

where $\lambda_z^2 \geq \lambda_y^2 \geq \lambda_x^2$.

The relative shape anisotropy κ^2 is calculated as:

$$\kappa^2 = \frac{3}{2}\frac{\lambda_x^4 + \lambda_y^4 + \lambda_z^4}{\left(\lambda_x^2 + \lambda_y^2 + \lambda_z^2\right)^2} - \frac{1}{2} \tag{B.2}$$

Appendix C. Supplementary material

Supplementary material related to this article can be found online at https://doi.org/10.1016/j.jcis.2023.05.057.

References

[1] J. Falbe (Ed.), Surfactants in Consumer Products, Springer, Berlin, Heidelberg, 1987.
[2] I. Kralova, J. Sjöblom, Surfactants used in food industry: a review, J. Dispers. Sci. Technol. 30 (2009) 1363–1383, https://doi.org/10.1080/01932690902735561.
[3] U. Kauscher, M.N. Holme, M. Björnmalm, M.M. Stevens, Physical stimuli-responsive vesicles in drug delivery: beyond liposomes and polymersomes, Adv. Drug Deliv. Rev. 138 (2019) 259–275, https://doi.org/10.1016/j.addr.2018.10.012.
[4] J.M. Neugebauer, [18] Detergents: an overview, in: M.P. Deutscher (Ed.), Methods in Enzymology, in: Guide to Protein Purification, vol. 182, Academic Press, 1990, pp. 239–253.
[5] A. Patist, J.R. Kanicky, P.K. Shukla, D.O. Shah, Importance of micellar kinetics in relation to technological processes, J. Colloid Interface Sci. 245 (2002) 1–15, https://doi.org/10.1006/jcis.2001.7955.
[6] E.A.G. Aniansson, S.N. Wall, Kinetics of step-wise micelle association, J. Phys. Chem. 78 (1974) 1024–1030, https://doi.org/10.1021/j100603a016.
[7] E.A.G. Aniansson, S.N. Wall, M. Almgren, H. Hoffmann, I. Kielmann, W. Ulbricht, R. Zana, J. Lang, C. Tondre, Theory of the kinetics of micellar equilibria and quantitative interpretation of chemical relaxation studies of micellar solutions of ionic surfactants, J. Phys. Chem. 80 (1976) 905–922, https://doi.org/10.1021/j100550a001.
[8] P.V. Coveney, J.A.D. Wattis, Analysis of a generalized Becker-Doring model of self-reproducing micelles, Proc. R. Soc., Math. Phys. Eng. Sci. 452 (1996) 2079–2102.
[9] J.A.D. Wattis, P.V. Coveney, Mesoscopic models of nucleation and growth processes: a challenge to experiment, Phys. Chem. Chem. Phys. 1 (1999) 2163–2176, https://doi.org/10.1039/A809348B.
[10] T. Taddese, R.L. Anderson, D.J. Bray, P.B. Warren, Recent advances in particle-based simulation of surfactants, Curr. Opin. Colloid Interface Sci. 48 (2020) 137–148, https://doi.org/10.1016/j.cocis.2020.04.001.
[11] A.K. Shchekin, I.A. Babintsev, L.T. Adzhemyan, Full-time kinetics of self-assembly and disassembly in micellar solution via the generalized Smoluchowski equation

with fusion and fission of surfactant aggregates, J. Chem. Phys. 145 (2016) 174105, https://doi.org/10.1063/1.4966233.
[12] I.M. Griffiths, C.J.W. Breward, D.M. Colegate, P.J. Dellar, P.D. Howell, C.D. Bain, A new pathway for the re-equilibration of micellar surfactant solutions, Soft Matter 9 (2012) 853–863, https://doi.org/10.1039/C2SM27154K.
[13] M. Kahlweit, Kinetics of formation of association colloids, J. Colloid Interface Sci. 90 (1982) 92–99, https://doi.org/10.1016/0021-9797(82)90401-5.
[14] E.E. Dormidontova, Micellization kinetics in block copolymer solutions: scaling model, Macromolecules 32 (1999) 7630–7644, https://doi.org/10.1021/ma9809029.
[15] R. Pool, P.G. Bolhuis, Prediction of an autocatalytic replication mechanism for micelle formation, Phys. Rev. Lett. 97 (2006) 018302, https://doi.org/10.1103/PhysRevLett.97.018302.
[16] S.J. Marrink, D.P. Tieleman, A.E. Mark, Molecular dynamics simulation of the kinetics of spontaneous micelle formation, J. Phys. Chem. B 104 (2000) 12165–12173, https://doi.org/10.1021/jp001898h.
[17] J.-B. Maillet, V. Lachet, P.V. Coveney, Large scale molecular dynamics simulation of self-assembly processes in short and long chain cationic surfactants, Phys. Chem. Chem. Phys. 1 (1999) 5277–5290, https://doi.org/10.1039/A905216J.
[18] M. Velinova, D. Sengupta, A.V. Tadjer, S.-J. Marrink, Sphere-to-rod transitions of nonionic surfactant micelles in aqueous solution modeled by molecular dynamics simulations, Langmuir 27 (2011) 14071–14077, https://doi.org/10.1021/la203055t.
[19] M. Jorge, Molecular dynamics simulation of self-assembly of n-decyltrimethylammonium bromide micelles, Langmuir 24 (2008) 5714–5725, https://doi.org/10.1021/la800291p.
[20] Z. Li, E.E. Dormidontova, Kinetics of diblock copolymer micellization by dissipative particle dynamics, Macromolecules 43 (2010) 3521–3531, https://doi.org/10.1021/ma902860j.
[21] H.B. Kolli, A. de Nicola, S.L. Bore, K. Schäfer, G. Diezemann, J. Gauss, T. Kawakatsu, Z.-Y. Lu, Y.-L. Zhu, G. Milano, M. Cascella, Hybrid particle-field molecular dynamics simulations of charged amphiphiles in an aqueous environment, J. Chem. Theory Comput. 14 (2018) 4928–4937, https://doi.org/10.1021/acs.jctc.8b00466.
[22] K. Schäfer, H.B. Kolli, M. Killingmoe Christensen, S.L. Bore, G. Diezemann, J. Gauss, G. Milano, R. Lund, M. Cascella, Supramolecular packing drives morphological transitions of charged surfactant micelles, Angew. Chem. Int. Ed. 59 (2020) 18591–18598, https://doi.org/10.1002/anie.202004522.
[23] P. Brown, C.P. Butts, J. Eastoe, Stimuli-responsive surfactants, Soft Matter 9 (2013) 2365–2374, https://doi.org/10.1039/C3SM27716J.
[24] T. Hayashita, T. Kurosawa, T. Miyata, K. Tanaka, M. Igawa, Effect of structural variation within cationic azo-surfactant upon photoresponsive function in aqueous solution, Colloid Polym. Sci. 272 (1994) 1611–1619, https://doi.org/10.1007/BF00664729.
[25] E. Chevallier, A. Mamane, H.A. Stone, C. Tribet, F. Lequeux, C. Monteux, Pumping-out photo-surfactants from an air–water interface using light, Soft Matter 7 (2011) 7866–7874, https://doi.org/10.1039/C1SM05378G.
[26] E. Chevallier, C. Monteux, F. Lequeux, C. Tribet, Photofoams: remote control of foam destabilization by exposure to light using an azobenzene surfactant, Langmuir 28 (2012) 2308–2312, https://doi.org/10.1021/la204200z.
[27] J. Royes, V.A. Bjørnestad, G. Brun, T. Narayanan, R. Lund, C. Tribet, Transition kinetics of mixed lipid: photosurfactant assemblies studied by time-resolved small angle X-ray scattering, J. Colloid Interface Sci. 610 (2022) 830–841, https://doi.org/10.1016/j.jcis.2021.11.133.
[28] C. Blayo, J.E. Houston, S.M. King, R.C. Evans, Unlocking structure–self-assembly relationships in cationic azobenzene photosurfactants, Langmuir 34 (2018) 10123–10134, https://doi.org/10.1021/acs.langmuir.8b02109.
[29] J. Eastoe, A. Vesperinas, Self-assembly of light-sensitive surfactants, Soft Matter 1 (2005) 338–347, https://doi.org/10.1039/B510877M.
[30] R. Lund, G. Brun, E. Chevallier, T. Narayanan, C. Tribet, Kinetics of photo-controllable micelles: light-induced self-assembly and disassembly of azobenzene-based surfactants revealed by TR-SAXS, Langmuir 32 (2016) 2539–2548, https://doi.org/10.1021/acs.langmuir.5b04711.
[31] J.C. Shelley, M.Y. Shelley, Computer simulation of surfactant solutions, Curr. Opin. Colloid Interface Sci. 5 (2000) 101–110, https://doi.org/10.1016/S1359-0294(00)00042-X.
[32] I.A. Silanteva, A.V. Komolkin, V.V. Mamontova, P.N. Vorontsov-Velyaminov, S. Santer, N.A. Kasyanenko, Some features of surfactant organization in DNA solutions at various NaCl concentrations, ACS Omega 5 (2020) 18234–18243, https://doi.org/10.1021/acsomega.0c01850.
[33] I.A. Silanteva, A.V. Komolkin, V.V. Mamontova, P.V. Gabrusenok, P.N. Vorontsov-Velyaminov, S. Santer, N.A. Kasyanenko, Cis-isomers of photosensitive cationic azobenzene surfactants in DNA solutions at different NaCl concentrations: experiment and modeling, J. Phys. Chem. B 125 (2021) 11197–11207, https://doi.org/10.1021/acs.jpcb.1c07864.
[34] L. Filipová, M. Kohagen, P. Štacko, E. Muchová, P. Slavíček, P. Klán, Photoswitching of azobenzene-based reverse micelles above and at subzero temperatures as studied by NMR and molecular dynamics simulations, Langmuir 33 (2017) 2306–2317, https://doi.org/10.1021/acs.langmuir.6b04455.
[35] E. Titov, A. Sharma, N. Lomadze, P. Saalfrank, S. Santer, M. Bekir, Photoisomerization of an azobenzene-containing surfactant within a micelle, ChemPhotoChem 5 (2021) 926–932, https://doi.org/10.1002/cptc.202100103.
[36] X. Liu, N.L. Abbott, Spatial and temporal control of surfactant systems, J. Colloid Interface Sci. 339 (2009) 1–18, https://doi.org/10.1016/j.jcis.2009.07.006.
[37] S. Peng, Q. Guo, P.G. Hartley, T.C. Hughes, Azobenzene moiety variation directing self-assembly and photoresponsive behavior of azo-surfactants, J. Mater. Chem. C 2 (2014) 8303–8312, https://doi.org/10.1039/C4TC00321G.
[38] P.-c. Chen, J.S. Hub, Validating solution ensembles from molecular dynamics simulation by wide-angle X-ray scattering data, Biophys. J. 107 (2014) 435–447, https://doi.org/10.1016/j.bpj.2014.06.006.
[39] C.J. Knight, J.S. Hub, WAXSiS: a web server for the calculation of SAXS/WAXS curves based on explicit-solvent molecular dynamics, Nucleic Acids Res. 43 (2015) W225–W230, https://doi.org/10.1093/nar/gkv309.
[40] W.L. Jorgensen, D.S. Maxwell, J. Tirado-Rives, Development and testing of the OPLS all-atom force field on conformational energetics and properties of organic liquids, J. Am. Chem. Soc. 118 (1996) 11225–11236, https://doi.org/10.1021/ja9621760.
[41] M.J. Abraham, T. Murtola, R. Schulz, S. Páll, J.C. Smith, B. Hess, E. Lindahl, GROMACS: high performance molecular simulations through multi-level parallelism from laptops to supercomputers, SoftwareX 1–2 (2015) 19–25, https://doi.org/10.1016/j.softx.2015.06.001.
[42] V. Vasudevan, S.H. Mushrif, Force field parameters for N,N-dimethylformamide (DMF) revisited: improved prediction of bulk properties and complete miscibility in water, J. Mol. Liq. 206 (2015) 338–342, https://doi.org/10.1016/j.molliq.2015.03.004.
[43] B. Hess, H. Bekker, H.J.C. Berendsen, J.G.E.M. Fraaije, LINCS: a linear constraint solver for molecular simulations, J. Comput. Chem. 18 (1997) 1463–1472, https://doi.org/10.1002/(SICI)1096-987X(199709)18:12<1463::AID-JCC4>3.0.CO;2-H.
[44] G. Bussi, D. Donadio, M. Parrinello, Canonical sampling through velocity rescaling, J. Chem. Phys. 126 (2007) 014101, https://doi.org/10.1063/1.2408420.
[45] M. Parrinello, A. Rahman, Polymorphic transitions in single crystals: a new molecular dynamics method, J. Appl. Phys. 52 (1981) 7182–7190, https://doi.org/10.1063/1.328693.
[46] J.S. Hub, B.L. de Groot, D. van der Spoel, g_wham—a free weighted histogram analysis implementation including robust error and autocorrelation estimates, J. Chem. Theory Comput. 6 (2010) 3713–3720, https://doi.org/10.1021/ct100494z.
[47] H. Heinz, R.A. Vaia, H. Koerner, B.L. Farmer, Photoisomerization of azobenzene grafted to layered silicates: simulation and experimental challenges, Chem. Mater. 20 (2008) 6444–6456, https://doi.org/10.1021/cm801287d.
[48] R. Biehl, Jscatter, a program for evaluation and analysis of experimental data, PLoS ONE 14 (2019) e0218789, https://doi.org/10.1371/journal.pone.0218789.
[49] S. Kawada, K. Fujimoto, N. Yoshii, S. Okazaki, Molecular dynamics study of the potential of mean force of SDS aggregates, J. Chem. Phys. 147 (2017) 084903, https://doi.org/10.1063/1.4998549.
[50] K. Fujimoto, Y. Kubo, S. Kawada, N. Yoshii, S. Okazaki, Molecular dynamics study of the aggregation rate for zwitterionic dodecyldimethylamine oxide and cationic dodecyltrimethylammonium chloride micelles, Mol. Simul. 43 (2017) 1331–1337, https://doi.org/10.1080/08927022.2017.1328557.
[51] M. Ledum, S. Sen, X. Li, M. Carrer, Y. Feng, M. Cascella, S.L. Bore, HyllerAasMD: a domain decomposition-based hybrid particle-field software for multi-scale simulations of soft matter, J. Chem. Theory Comput. (2023), in press, https://doi.org/10.26434/chemrxiv-2021-796ql.
[52] S.L. Bore, M. Cascella, Hamiltonian and alias-free hybrid particle–field molecular dynamics, J. Chem. Phys. 153 (2020) 094106, https://doi.org/10.1063/5.0020733.
[53] P.C. Hiemenz, R. Rajagopalan, Principles of Colloid and Surface Chemistry, Revised and Expanded, 3rd edition, CRC Press, 1997.
[54] S. Bhattacharjee, M. Elimelech, M. Borkovec, DLVO interaction between colloidal particles: beyond Derjaguin's approximation, Croat. Chem. Acta 71 (1998) 883–903.
[55] R. Lund, L. Willner, D. Richter, Kinetics of block copolymer micelles studied by small-angle scattering methods, in: A. Abe, K.-S. Lee, L. Leibler, S. Kobayashi (Eds.), Controlled Polymerization and Polymeric Structures: Flow Microreactor Polymerization, Micelles Kinetics, Polypeptide Ordering, Light Emitting Nanostructures, in: Advances in Polymer Science, Springer International Publishing, Cham, 2013, pp. 51–158.
[56] B. Wen, B. Bai, R.G. Larson, Surfactant desorption and scission free energies for cylindrical and spherical micelles from umbrella-sampling molecular dynamics simulations, J. Colloid Interface Sci. 599 (2021) 773–784, https://doi.org/10.1016/j.jcis.2021.04.138.
[57] B.C. Stephenson, K.A. Stafford, K.J. Beers, D. Blankschtein, Application of computer simulation free-energy methods to compute the free energy of micellization as a function of micelle composition. 1. Theory, J. Phys. Chem. B 112 (2008) 1634–1640, https://doi.org/10.1021/jp0727603.
[58] F. Yuan, S. Wang, R.G. Larson, Potentials of mean force and escape times of surfactants from micelles and hydrophobic surfaces using molecular dynamics simulations, Langmuir 31 (2015) 1336–1343, https://doi.org/10.1021/la5044393.
[59] K. Bernardino, A.F. de Moura, Aggregation thermodynamics of sodium octanoate micelles studied by means of molecular dynamics simulations, J. Phys. Chem. B 117 (2013) 7324–7334, https://doi.org/10.1021/jp312840y.
[60] B.J. Chun, J.I. Choi, S.S. Jang, Molecular dynamics simulation study of sodium dodecyl sulfate micelle: water penetration and sodium dodecyl sulfate dissociation, Colloids Surf. A, Physicochem. Eng. Asp. 474 (2015) 36–43, https://doi.org/10.1016/j.colsurfa.2015.03.002.

[61] Y. Rharbi, M. Karrouch, P. Richardson, Fusion and fission inhibited by the same mechanism in electrostatically charged surfactant micelles, Langmuir 30 (2014) 7947–7952, https://doi.org/10.1021/la501465v.
[62] A. Patist, B.K. Jha, S.-G. Oh, D.O. Shah, Importance of micellar relaxation time on detergent properties, J. Surfactants Deterg. 2 (1999) 317–324, https://doi.org/10.1007/s11743-999-0083-6.
[63] C. Herdes, E.E. Santiso, C. James, J. Eastoe, E.A. Müller, Modelling the interfacial behaviour of dilute light-switching surfactant solutions, J. Colloid Interface Sci. 445 (2015) 16–23, https://doi.org/10.1016/j.jcis.2014.12.040.
[64] H. Ishkhanyan, N.H. Rhys, D.J. Barlow, M.J. Lawrence, C.D. Lorenz, Impact of drug aggregation on the structural and dynamic properties of Triton X-100 micelles, Nanoscale 14 (2022) 5392–5403, https://doi.org/10.1039/D1NR07936K.
[65] M. He, W. Zheng, N. Wang, H. Gao, D. Ouyang, Z. Huang, Molecular dynamics simulation of drug solubilization behavior in surfactant and cosolvent injections, Pharmaceutics 14 (2022) 2366, https://doi.org/10.3390/pharmaceutics14112366.
[66] A.C. Hamill, S.-C. Wang, C.T. Lee, Solution structure of an amyloid-forming protein during photoinitiated hexamer-dodecamer transitions revealed through small-angle neutron scattering, Biochemistry 46 (2007) 7694–7705, https://doi.org/10.1021/bi700233k.
[67] C.T. Lee, K.A. Smith, T.A. Hatton, Photocontrol of protein folding: the interaction of photosensitive surfactants with bovine serum albumin, Biochemistry 44 (2005) 524–536, https://doi.org/10.1021/bi048556c.
[68] C.T. Lee, K.A. Smith, T.A. Hatton, Photoreversible viscosity changes and gelation in mixtures of hydrophobically modified polyelectrolytes and photosensitive surfactants, Macromolecules 37 (2004) 5397–5405, https://doi.org/10.1021/ma036019e.
[69] A.-L.M. Le Ny, C.T. Lee, Photoreversible DNA condensation using light-responsive surfactants, J. Am. Chem. Soc. 128 (2006) 6400–6408, https://doi.org/10.1021/ja0576738.
[70] H. Asanuma, T. Ito, T. Yoshida, X. Liang, M. Komiyama, Photoregulation of the formation and dissociation of a DNA duplex by using the cis–trans isomerization of azobenzene, Angew. Chem. Int. Ed. 38 (1999) 2393–2395, https://doi.org/10.1002/(SICI)1521-3773(19990816)38:16<2393::AID-ANIE2393>3.0.CO;2-7.